

NoLimits.jl: Flexible and Composable Nonlinear Mixed-Effects Modeling in Julia

Manuel Huth^{1,2}, Jonas Arruda^{1,2}, Nina Schmid^{1,2}, Roy Gusinow^{1,2},
Vincent Wieland^{1,2}, Clemens Peiter^{1,2}, and Jan Hasenauer^{1,2,*}

¹ Life and Medical Sciences (LIMES) Institute, University of Bonn, Bonn, Germany

² Bonn Center for Mathematical Life Sciences, University of Bonn, Bonn, Germany

* Corresponding author (jan.hasenauer@uni-bonn.de)

Abstract

Nonlinear mixed-effects models are widely used to analyze longitudinal data, but existing open-source software often supports only a limited subset of the model structures, inference methods, machine-learning components, automatic differentiation techniques, and random-effects distributions required in modern applications. We introduce **NoLimits.jl**, an open-source Julia package for flexible and composable nonlinear mixed-effects modeling. Its macro-based modeling language enables observation and latent-state models to be constructed from diverse building blocks, including ordinary differential equations, Markov models, and neural networks. **NoLimits.jl** supports flexible, covariate-dependent observation and random-effects distributions and provides a unified interface to frequentist inference through Laplace approximation, stochastic expectation maximization, and Bayesian Markov chain Monte Carlo methods. We demonstrate the package on three case studies showcasing its workflows, integration of differentiable machine-learning components, and data-driven estimation of random-effects distributions using normalizing flows. Together, these capabilities substantially expand the range of nonlinear mixed-effects models that can be specified, estimated, and compared within a single open-source framework.

Keywords: nonlinear mixed-effects models, longitudinal data analysis, scientific machine learning, normalizing flows, Julia.

1 Introduction

Nonlinear mixed-effects (NLME) models are a central tool across a wide range of scientific domains, including pharmacometrics [Mould and Upton, 2012, Gobburu, 2010], clinical data [Maheux et al., 2023, Cogswell et al., 2023], systems biology [Karlsson et al., 1995, Fröhlich et al., 2017], psychometrics [Rijmen et al., 2003, Chung and Cai, 2021], and ecology [Schliehe-Diecks et al., 2012, Muff et al., 2020]. Such studies generate repeated measurements from multiple individuals, whose responses often vary substantially due to both observed and unobserved sources of heterogeneity [Lavielle, 2014, Pinheiro et al., 2007]. Throughout this article, we use the term *individual* generically to denote any experimental unit with repeated observations, including humans, animals, cells, countries, or other subjects under study. NLMEs address the variability by combining a population-level model with individual-specific random effects, enabling the joint estimation of population characteristics and individual deviations. Their hierarchical structure further supports the integration of sophisticated model components, ranging from mechanistic systems such as differential equations [Mould and Upton, 2012] to machine-learning-based approaches [Ngufor et al., 2019, Sigrist, 2022]. Moreover, we view hierarchical Bayesian models as NLME models, with the Bayesian formulation differing primarily by the use of prior distributions and posterior inference [Gelman et al., 2013].

At the same time, the complexity of models used in practice has grown substantially. Modern applications increasingly integrate mechanistic models with neural networks [Rackauckas et al., 2020b], particularly in fields such as neuroscience [El-Gazzar and van Gerven, 2025] and systems biology [Philipps et al., 2025], as well as with other differentiable machine-learning components [Wörtwein et al., 2023]. While these developments expand the range of problems that can be represented, they also introduce new computational challenges which need to be addressed by scientific software. Researchers require frameworks that can integrate different model components, probability distributions, and inference algorithms within a unified workflow, while remaining compatible with modern automatic differentiation and machine-learning ecosystems.

Existing software systems differ substantially in their modeling abstractions, inference capabilities, extensibility, and open-source availability. General mixed-effects frameworks such as **nlme** [Pinheiro and Bates, 2000] and **lme4** [Bates et al., 2015] primarily target reduced-form mixed-effects formulations and do not natively support mechanistic ordinary differential equation (ODE) systems or Markov models and are focused on Gaussian random effects. Dedicated NLME software, including proprietary platforms such as **NONMEM** [Bauer, 2019], **Monolix** [Simulations Plus, 2024], and **Pumas** [Rackauckas et al., 2020b], as well as open-source alternatives such as **nlmixr2** [Fidler, 2025] and **saemix** [Comets et al., 2017], provides specialized workflows for ODE-based mechanistic modeling. However, support for Markov-model and latent-state formulations remains comparatively limited in these frame-

works. Specialized tools such as **mHMMbayes** [Aarts and Mildiner Moraga, 2026] instead focus specifically on hierarchical hidden Markov models (HMMs). In parallel, probabilistic programming frameworks such as **Stan** [Stan Development Team, 2026], **Turing.jl** [Ge et al., 2018, Fjelde et al., 2025], and **PyMC** [Abril-Pla et al., 2023] offer flexible Bayesian inference workflows and allow users to define custom hierarchical ODE and latent-state models, but they often require substantial manual implementation of NLME-specific workflows.

These frameworks also differ in their support of standard inference procedures. **NONMEM** and **nlmixr2** support estimation by the stochastic approximation expectation maximization (SAEM) [Wei and Tanner, 1990, Kuhn and Lavielle, 2004] and first-order conditional estimation with interaction (FOCEI) [Pinheiro and Chao, 2006, Wang, 2007], whereas **Monolix** and **saemix** are centered on SAEM estimation. The probabilistic programming languages **Stan**, **Turing.jl**, and **PyMC** emphasize Bayesian Markov chain Monte Carlo (MCMC) and variational-inference approaches [Blei et al., 2017]. Among dedicated NLME frameworks, **Pumas** provides one of the broadest collections of inference paradigms, including FOCEI-, Laplace-, and SAEM-based methods, as well as variational and Bayesian workflows.

Beyond model classes and inference algorithms, frameworks vary substantially in their support for random effects distributions and integration with machine-learning libraries. In many classical NLME frameworks, including **Monolix**, **saemix**, and **nlmixr2**, support for heavy-tailed or user-defined random-effects distributions remains limited, while **Pumas** offers greater flexibility. **Pumas**, **Turing.jl**, and **PyMC** provide more composable interfaces to modern neural-network ecosystems and automatic differentiation, whereas neural-network-based models in frameworks such as **NONMEM** and **Monolix** often require manual specification of network architectures [Bräm et al., 2025].

These limitations highlight the need for open-source NLME frameworks that support diverse model classes and inference procedures while remaining compatible with modern automatic differentiation and machine-learning ecosystems. To the best of our knowledge, no existing open-source framework provides this combination of capabilities, and in particular none enables the integration of mixed HMMs with a diverse range of built-in neural network components.

To address these limitations, we introduce **NoLimits.jl** (**Non Linear Mixed Effects.jl**), an open-source framework for flexible nonlinear mixed-effects modeling in **Julia** [Bezanson et al., 2017]. **NoLimits.jl** unifies mechanistic modeling, statistical inference, and scientific machine learning within a common modeling and inference framework. In **NoLimits.jl**, mechanistic terms, machine-learning components, and custom distributions can be composed into a single model definition combining fixed effects, random effects, and structural and observation models. Point-estimation and uncertainty-quantification can be conducted with various methods and the fitted model assessed with goodness-of-fit, random-effect-specific, and model-comparison tools (Figure 1).

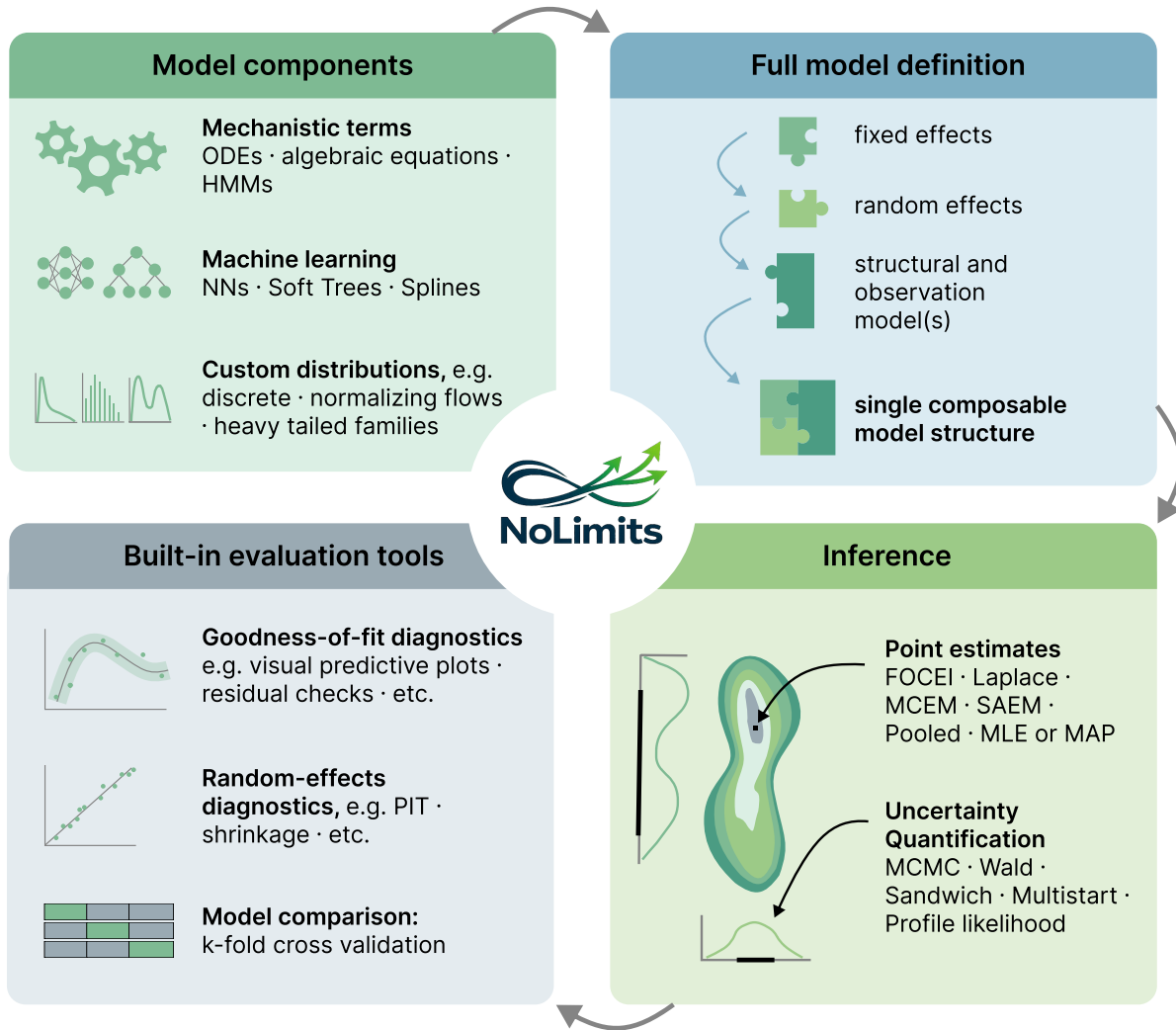


Figure 1: Overview of the **NoLimits.jl** workflow. Mechanistic terms, machine-learning components, and custom distributions are combined into a single composable model structure comprising fixed effects, random effects, and structural and observation models. Inference yields estimates for fixed and random effects, optionally including uncertainty quantification. Built-in evaluation tools support model validation, comparison, and diagnostic assessment, guiding potential revisions to the selected model components.

The core modeling abstraction in **NoLimits.jl** represents observation models as parameterized conditional distributions and that inference is decoupled from model specification. The capabilities of **NoLimits.jl** can be broadly divided into three areas: flexible model specification, integration with the Julia scientific machine-learning ecosystem, and support for a wide range of inference procedures.

Flexible model specification in **NoLimits.jl** naturally encompasses a broad range of longitudinal models, including mechanistic models such as ODE systems [Hartman, 2002] and discrete-

and continuous-time Markov models with hidden or observed states [Rabiner, 1989, Zucchini et al., 2016], differentiable machine-learning models such as neural networks [Goodfellow et al., 2016, Hornik et al., 1989] and soft trees [Irsoy et al., 2012], hybrid mechanistic–neural models [Rackauckas et al., 2020a], and joint models with multiple observation types. To support these diverse model classes, **NoLimits.jl** provides a macro-based language for composing observation models and latent structures from rich model components and probability distributions. This includes the rich collection of distributions available through **Distributions.jl** [Besançon et al., 2021], including heavy-tailed distributions. The random-effects distribution can likewise be chosen flexibly from the **Distributions.jl** ecosystem, also including univariate and multivariate, heavy-tailed, and normalizing flows [Rezende and Mohamed, 2015] for flexible distributional modeling, provided through **NormalizingFlows.jl** [Ge et al., 2018, Fjelde et al., 2025]. In addition, the parameters of the random-effects distribution may depend on covariates through arbitrary differentiable functions, allowing the specification of both known and previously unknown covariate–random-effects relationships.

The second capability area is tight integration with the **Julia** scientific computing ecosystem, enabling **NoLimits.jl** to use established tools for machine learning, differential equations, optimization, and automatic differentiation. Neural-network-based model components can be implemented directly using **Lux.jl** [Pal, 2023] or **SimpleChains.jl** [PumasAI, 2022], enabling neural structural models, observation mappings, and random-effects distributions. Differentiable soft decision trees are additionally available as interpretable function approximators for each of these components. Mechanistic models leverage the SciML ecosystem through **OrdinaryDiffEq.jl** [Rackauckas and Nie, 2017], providing access to differentiable ODE solvers, event handling, and callback mechanisms. Automatic differentiation is supported through **ForwardDiff.jl** [Revels et al., 2016], while numerical optimization is provided by **Optimization.jl** [Dixit and Rackauckas, 2023], including optimizers from **Optimisers.jl** [Innes, 2018] that are widely used in machine-learning applications.

The third capability area is support for a broad range of inference procedures through a common interface. These include Laplace-based approximation methods, stochastic expectation maximization (EM) algorithms such as SAEM and Monte Carlo expectation maximization (MCEM), and Bayesian inference via MCMC methods. Additionally, users can specify fixed-effects-only models and estimate parameters for them via maximum likelihood (MLE), MCMC, or variational inference methods through **Turing.jl**. Because inference is decoupled from model specification, users can switch between estimation procedures with minimal changes to the analysis workflow, facilitating direct comparisons of alternative inference strategies under a common model.

NoLimits.jl is released as open-source software under the MIT license and is developed publicly at github.com/manuhuth/NoLimits.jl, with documentation available at manuhuth.github.io/NoLimits.jl. The latest stable version can be installed from the Julia reposi-

tory using the package manager.

```
using Pkg
Pkg.add("NoLimits")
```

The package requires Julia 1.12 or later and can be installed using `Pkg.add`.

The remainder of this article is organized as follows. Section 2 reviews the NLME modeling framework together with the estimation, uncertainty quantification, prediction, and evaluation methods underlying **NoLimits.jl**. Sections 3, 4, and 5 describe model specification using the `@Model` macro, parameter estimation through a unified inference interface, and uncertainty quantification and model diagnostics, respectively. Section 6 demonstrates the framework on three case studies: an ODE model of warfarin pharmacokinetics, a learnable concentration-effect function for warfarin pharmacodynamics, and a normalizing flow as a flexible random-effects distribution for fish growth. Section 7 compares **NoLimits.jl** with existing software frameworks, and Section 8 concludes.

2 Nonlinear mixed-effects models

In the following, we review the NLME model class on which **NoLimits.jl** is built. We present the frequentist formulation first and add the Bayesian perspective as an extension in Section 2.8. For clarity, we present the framework using a single grouping level, with one random-effect vector per individual and a single, uncensored observation. The formulation extends naturally to multiple nested and crossed grouping levels (Appendix A.1), multiple observation types per individual (Appendix A.2), and censored observations (Appendix A.3).

2.1 The frequentist’s mixed-effects model

We begin with the frequentist formulation, in which the population parameters are fixed unknowns shared across all individuals. Individuals are indexed by $i = 1, \dots, N$, where N is the total number of individuals, and observations within individual i are indexed by $j = 1, \dots, n_i$, where n_i is the number of observations for individual i . Both the number and timing of observations may vary across individuals.

2.1.1 Hierarchical generative model.

Let $\theta \in \Theta \subseteq \mathbb{R}^{n_\theta}$ denote the population parameters shared across all individuals, and let $x_i \in \mathbb{R}^{n_{x_i}}$ denote the time-invariant covariates of individual i . The data-generating process

is assumed to consist of two levels [Lindstrom and Bates, 1990, Pinheiro et al., 2007],

$$B_i \sim p_B(\cdot | x_i, \theta), \tag{1}$$

$$Y_i | B_i = b \sim p_{Y|B}(\cdot | b, x_i, \theta), \tag{2}$$

where B_i is the random-effect vector of individual i , taking values in the support $\mathcal{B} \subseteq \mathbb{R}^{n_b}$ with density $p_B(b | x_i, \theta)$, and Y_i is the response vector of individual i , taking values in the support $\mathcal{Y}_i \subseteq \mathbb{R}^{n_i}$. Conditional on B_i , the response is distributed according to the observation density $p_{Y|B}(y | b, x_i, \theta)$. We write $b_i \in \mathcal{B}$ and $y_i \in \mathcal{Y}_i$ for realizations of B_i and Y_i , respectively. Observations are, conditionally on covariates, assumed independent across individuals, whereas observations within an individual are correlated through the shared random effect B_i and the conditional joint distribution $p_{Y|B}(\cdot | b, x_i, \theta)$. As outlined in the notation, the random-effects distribution may depend on individual-fixed covariates x_i , allowing individual heterogeneity modeled by random effects to vary according to baseline characteristics.

2.1.2 Flexibility of the conditional model.

The hierarchical formulation in Equations 1 and 2 restricts the conditional model $p_{Y|B}(y | b, x, \theta)$ only by requiring its density to be evaluable, so observation distributions may be continuous, binary, count, or censored, with multiple observations of different types modeled jointly for the same individual. The structural model itself may be a closed-form expression, the solution of a system of ODEs, the initial, transition or emission structure of a Markov model with hidden or observed states, or a differentiable machine-learning model such as a neural network or soft tree, and subject to mild technical conditions these components combine freely within a single model. **NoLimits.jl** implements all of these structural forms through a common model syntax (Section 3).

2.1.3 Flexibility of the random-effect distribution.

The random-effects distribution is specified independently of the observation model. In addition to the multivariate Gaussian and log-normal families commonly used in NLME modeling, the formulation accommodates arbitrary continuous univariate or multivariate distributions, including heavy-tailed and skewed families such as the Student's t , beta, χ^2 , and exponential distributions, as well as user-defined distributions and normalizing flows [Rezende and Mohamed, 2015], which construct complex probability distributions by transforming a simple base distribution through a sequence of invertible differentiable mappings whose parameters are learned from data [Rezende and Mohamed, 2015, Papamakarios et al., 2021], enabling flexible random-effects distributions to be learned from data. In **NoLimits.jl**, we

draw standard parametric families from **Distributions.jl** and use learnable normalizing flows for distributions estimated from data (Section 3).

For normalizing flows, the random effect is generated as $B_i = T_\psi(U_i)$, where $U_i \sim p_U$ is a base random variable, typically a multivariate standard Gaussian, and T_ψ is an invertible differentiable transformation with parameters ψ . The corresponding density follows from the change-of-variables formula,

$$p_B(b \mid \psi) = p_U(T_\psi^{-1}(b)) \left| \det \nabla_b T_\psi^{-1}(b) \right|, \quad (3)$$

yielding a tractable likelihood in which ψ can be estimated jointly with the remaining model parameters [Rezende and Mohamed, 2015, Papamakarios et al., 2021]. Section 6.3 illustrates this approach using planar flows, which compose multiple such transformations [Rezende and Mohamed, 2015].

2.2 Joint and marginal likelihood

The hierarchical structure in Equations 1 and 2 induces the factorization

$$p_{Y,B}(y_i, b_i \mid x_i, \theta) = p_{Y|B}(y_i \mid b_i, x_i, \theta) p_B(b_i \mid x_i, \theta), \quad (4)$$

which defines the joint density of the response and random effects for individual i . When viewed as a function of θ , this quantity is commonly referred to as the *complete-data likelihood*. If the random effects were observed, inference would be based directly on the corresponding complete-data log-likelihood,

$$\ell_c(\theta) = \sum_{i=1}^N \log p_{Y,B}(y_i, b_i \mid x_i, \theta), \quad (5)$$

which would be straightforward to evaluate.

In practice, however, the random effects are latent and therefore unobserved. Inference must instead be based on the marginal distribution of the observed responses, obtained by integrating the random effects out of the joint density [Dempster et al., 1977, Lindstrom and Bates, 1990],

$$p_Y(y_i \mid x_i, \theta) = \int_{\mathcal{B}} p_{Y|B}(y_i \mid b, x_i, \theta) p_B(b \mid x_i, \theta) db, \quad (6)$$

where we assume that the integral exists for every $\theta \in \Theta$ [Pinheiro and Bates, 1995]. Under independence across individuals, the population parameters are estimated by maximizing the marginal log-likelihood

$$\hat{\theta} = \arg \max_{\theta \in \Theta} \ell(\theta), \quad \ell(\theta) = \sum_{i=1}^N \log p_Y(y_i \mid x_i, \theta), \quad (7)$$

or, equivalently, by minimizing the negative marginal log-likelihood.

For many practically relevant models, the integral in Equation 6 is not available in closed form. This occurs, for example, when the conditional model is nonlinear in the random effects, or non-Gaussian observation distributions are used [Pinheiro and Bates, 1995, Lindstrom and Bates, 1990]. Consequently, the marginal log-likelihood in Equation 7 is often intractable, and estimation methods must approximate the marginal integral. The approaches described in Section 2.4 differ primarily in how this approximation is performed, through repeated evaluations, approximations, or expectations involving the complete-data likelihood in Equation 4. In **NoLimits.jl**, a model specification determines this joint density directly, and the estimators of Section 4 form the approximations to the otherwise intractable marginal likelihood.

2.3 Empirical Bayes estimates

Although inference for the population parameters is based on the marginal likelihood in Equation 7, many applications additionally require individual-specific estimates of the latent random effects. These estimates are obtained from the conditional distribution of the random effects given the observed response of an individual. By Bayes' theorem applied to Equations 1 and 2, this distribution is given by

$$p_{B|Y}(b | y_i, x_i, \theta) \propto p_{Y|B}(y_i | b, x_i, \theta) p_B(b | x_i, \theta), \quad (8)$$

where the normalizing constant is the marginal density of Equation 6. The empirical Bayes estimate (EBE) [Lindstrom and Bates, 1990, Davidian and Giltinan, 2003] of the random effects for individual i is defined as the posterior mode,

$$\hat{b}_i(\theta) = \arg \max_{b \in \mathcal{B}} [\log p_{Y|B}(y_i | b, x_i, \theta) + \log p_B(b | x_i, \theta)]. \quad (9)$$

The EBE plays a central role throughout mixed-effects modeling. It serves as the expansion point for the Laplace and FOCEI approximations discussed in Section 2.4 and provides the individual-level predictions and residual diagnostics.

2.4 Point estimation

To address the challenge posed by the intractable integral in Equation 6, we review a spectrum of well-established estimation methods that trade computational cost against statistical accuracy: a pooled estimator that fixes the random effects and thus avoids integration over random effects, the deterministic Laplace and FOCEI approximations, and the stochastic MCEM and SAEM algorithms [Tierney and Kadane, 1986, Wang, 2007, Wei and Tanner,

1990, Delyon et al., 1999]. The following sections describe these methods, while the corresponding derivations are deferred to Appendix A.5, Appendix A.6, and Appendix A.8.

In **NoLimits.jl**, these estimators share a common fitting interface, so a single model specification can be moved between them, or chained from an inexpensive pooled fit to a Laplace, FOCEI, or SAEM refinement, without being rewritten (Section 4).

2.4.1 Pooled estimation.

As a computationally inexpensive baseline, one may ignore between-individual variability and estimate the population parameters using a pooled model. The classical naive pooled estimator treats all observations as arising from a single population and ignores inter-individual variability [Sheiner and Beal, 1980]. The classical naive pooled estimator treats all observations as arising from a single population and ignores inter-individual variability [Sheiner and Beal, 1980] by replacing each random effect with its conditional mean $\mu_{b_i} = \mathbb{E}(B_i | x_i, \theta)$ and maximizing the resulting population-level likelihood,

$$\hat{\theta} = \arg \max_{\theta \in \Theta} \sum_{i=1}^N \log p_{Y|B}(y_i | B = \mu_{b_i}, x_i, \theta). \quad (10)$$

For random-effects distributions without covariate effects, Equation 10 reduces to the classical naive pooled estimator.

Because no integration over random effects is required, pooled estimation is computationally inexpensive and can serve as an initializer for more sophisticated estimators or as a preliminary model check. Since between-individual variability is ignored, however, the parameters of the random-effects distribution $p_B(b | x_i, \theta)$ are generally not identifiable.

2.4.2 Laplace approximation.

The Laplace approximation replaces the marginal integral in Equation 6 by a second-order Taylor expansion of the log joint density around the EBE [Tierney and Kadane, 1986]. Because the gradient of the log joint density vanishes at the mode, the resulting quadratic approximation yields a Gaussian integral that can be evaluated analytically,

$$p_Y(y_i | x_i, \theta) \approx (2\pi)^{n_b/2} \det(-H_i(\theta))^{-1/2} p_{Y|B}(y_i | \hat{b}_i, x_i, \theta) p_B(\hat{b}_i | x_i, \theta), \quad (11)$$

where $\hat{b}_i = \hat{b}_i(\theta)$ is the EBE from Equation 9 and $H_i(\theta)$ is the Hessian of the log joint density with respect to b at \hat{b}_i . Each evaluation therefore requires both the EBE and its Hessian, and the approximation is accurate when the posterior of Equation 8 is close to Gaussian and the random-effects dimension n_b is moderate. A derivation, including bounded random-effect domains and the gradient of the approximate marginal log-likelihood via the envelope theorem, is given in Appendix A.5.

2.4.3 First-order conditional estimation with interaction.

FOCEI uses the same approximation as Equation 11 and differs only in its treatment of the curvature matrix $H_i(\theta)$. Instead of the exact Hessian, it employs a first-order linearization of the conditional model around the EBE, approximating the curvature of the conditional log-likelihood by its Fisher information [Fisher, 1925] while retaining the exact curvature of the random-effects distribution [Wang, 2007, Pinheiro and Chao, 2006]. As a result, it is often faster than the Laplace approximation and has become a standard method in pharmacometrics, although its accuracy may degrade when the conditional model is highly nonlinear in the random effects. The explicit curvature matrix and a derivation are provided in Appendix A.5.

2.4.4 Monte Carlo expectation maximization.

The EM algorithm avoids direct optimization of the marginal likelihood, alternating between an expectation and a maximization step [Dempster et al., 1977]. At iteration t with current estimate θ_t , the expectation step constructs the surrogate objective, Q , which is the posterior expectation of the complete-data log-likelihood of Equation 5 derived from the evidence lower bound (ELBO),

$$Q(\theta \mid \theta_t) = \sum_{i=1}^N \mathbb{E}_{B \sim p_{B|Y}(\cdot | y_i, x_i, \theta_t)} [\log p_{Y,B}(y_i, B \mid x_i, \theta)], \quad (12)$$

and the maximization step updates the parameters according to

$$\theta_{t+1} = \arg \max_{\theta \in \Theta} Q(\theta \mid \theta_t). \quad (13)$$

For nonlinear or non-Gaussian models, the expectation in Equation 12 is generally intractable because the posterior distribution in Equation 8 has no closed form. MCEM addresses this by replacing the expectation with a Monte Carlo average over samples drawn from the posterior using MCMC [Wei and Tanner, 1990]. Common choices include Metropolis–Hastings [Robert and Casella, 2004] and the no-U-turn sampler (NUTS) [Hoffman et al., 2014], with Metropolis–Hastings often serving as a natural default because it requires only evaluations of the joint density and no gradients of the conditional model. As the number of Monte Carlo samples increases across iterations, the limit points of the algorithm coincide with stationary points of the marginal log-likelihood. Unlike the exact EM algorithm, however, the stochastic expectation step does not guarantee monotonic improvement of the objective [Wei and Tanner, 1990]. Additional details on the sampling identities are provided in Appendix A.6.

2.4.5 Stochastic approximation expectation maximization.

For models in which each likelihood evaluation is expensive, for example when the conditional density requires solving an ODE, drawing a new Monte Carlo sample at every iteration is costly. SAEM instead maintains a running stochastic approximation of the surrogate [Delyon et al., 1999, Kuhn and Lavielle, 2004]. At iteration t it draws M_t samples $b_i^{(t,1)}, \dots, b_i^{(t,M_t)}$ from the posterior of Equation 8 and updates

$$Q^{(t)}(\theta) = (1 - \gamma_t) Q^{(t-1)}(\theta) + \gamma_t \sum_{i=1}^N \frac{1}{M_t} \sum_{s=1}^{M_t} \log p_{Y,B}(y_i, b_i^{(t,s)} | x_i, \theta), \quad (14)$$

where the step sizes $\{\gamma_t\}$ satisfy the Robbins–Monro conditions $\sum_t \gamma_t = \infty$ and $\sum_t \gamma_t^2 < \infty$. These conditions ensure, under suitable convergence conditions, convergence of the SAEM iterates [Delyon et al., 1999]. The schedule of Appendix A.7 is used in practice. When the complete-data model belongs to an exponential family, SAEM reduces to recursive updates of finite-dimensional sufficient statistics, followed by closed-form maximization steps [Kuhn and Lavielle, 2005, Comets et al., 2017]. Parameters that enter as natural parameters of the exponential family can be updated analytically, whereas parameters appearing in non-linear or neural components are optimized numerically. A single model fit can therefore combine closed-form and numerical updates. The sufficient-statistic formulation is derived in Appendix A.8.

2.5 Uncertainty quantification

While point estimation provides a single best-fitting value for each parameter, these estimates are associated with uncertainty because they are inferred from a finite and potentially noisy sample of data. In **NoLimits.jl**, we implemented three interval estimates for a likelihood-based fit, all evaluated at the maximum-likelihood estimate of Equation 7: Wald-type intervals based on the observed information matrix, a misspecification-robust variant based on the sandwich estimator, and profile-likelihood intervals. Their software interface is described in Section 5, and the Bayesian counterpart based on posterior samples is deferred to Section 2.8.

2.5.1 Wald-type and misspecification-robust intervals.

Wald-type intervals rely on the asymptotic normality of maximum-likelihood estimators [van der Vaart, 1998] and use the observed information matrix, the negative Hessian of the marginal log-likelihood of Equation 7 at the estimate, computed for the Laplace and FOCEI estimators from the approximated marginal log-likelihood of Equation 11 and likewise for MCEM and SAEM. Because the inverse observed information is valid only under correct model specification, the sandwich estimator [White, 1982] incorporates the empirical

covariance of the individual score contributions to provide misspecification-robust standard errors. When the information-matrix equality holds, it coincides with the inverse observed information matrix.

2.5.2 Profile-likelihood intervals.

Profile-likelihood intervals [Meeker and Escobar, 1995] avoid the normality assumption underlying Wald intervals by inverting the likelihood-ratio statistic of each parameter against a χ^2 threshold [Raue et al., 2009]. They are particularly useful for parameters with asymmetric uncertainty or estimates near the boundary of the parameter space, and they can reveal practical non-identifiability that Wald intervals often obscure. Their computation requires repeated constrained optimizations and can therefore become demanding for large models.

2.6 Prediction

Beyond estimating the population parameters and their uncertainty, a fitted model is used to predict responses, which in a mixed-effects model depends on whether the individual was observed during model fitting. For an individual included in the training data, the observed responses inform the posterior of the random effect in Equation 8, and a prediction at a covariate value or time point either substitutes the corresponding EBE into the conditional mean or averages the conditional mean over this posterior. For an individual not observed during fitting, no such posterior is available, and the prediction either plugs the covariate-dependent prior mean of the random effect into the conditional mean or integrates the conditional mean over the prior, the latter giving the population mean implied by the marginal model of Equation 6. Within each setting the two predictors coincide when the conditional mean is linear in the random effect and generally differ otherwise [Lindstrom and Bates, 1990, Lavielle, 2014]. The corresponding expressions are given in Appendix A.9. In **NoLimits.jl**, predictions for both observed and new individuals are available and supply the values used by its diagnostics and plots (Section 5).

2.7 Model evaluation

Because such predictions are only as trustworthy as the fit that produces them, a fitted model should be assessed for its absolute goodness of fit, the adequacy of the assumed random-effects distribution, its performance relative to competing specifications, and the reliability of both the individual estimates and the fit itself. In **NoLimits.jl**, we provide diagnostics and cross-validation for each of these aspects (Section 5).

2.7.1 Goodness-of-fit diagnostics.

The adequacy of the fitted model is assessed by comparing its predictions with the observed data. A visual predictive check (VPC) compares observed data quantiles with prediction intervals obtained from replicate datasets simulated under the fitted model [Bergstrand et al., 2011]. Residual diagnostics compare each observation with its population and individual predictions (population predictions (PRED) and individual predictions (IPRED), Equations 48 and 46). The weighted residual (weighted residuals (WRES)) [Hooker et al., 2007] standardizes the difference between an observation and its PRED by the corresponding predictive standard deviation. The probability integral transform (PIT) evaluates the fitted predictive cumulative distribution function at the observed value. Under correct model specification, the resulting values are uniformly distributed, and their standard-normal quantiles define normally distributed quantile residuals.

2.7.2 Random-effects diagnostics.

In addition to reproducing the observed responses, a mixed-effects model must adequately characterize between-individual variability through its random-effects distribution. This assumption is assessed using diagnostics based on the estimated random effects. The PIT of the EBEs under their fitted distribution is uniform when the random effects prior is correctly specified, summarized as per-coordinate PIT.

Shrinkage quantifies the extent to which an EBE is pulled toward the population mean when the data provide limited information about an individual. For each random-effect coordinate, the ETA shrinkage [Savic and Karlsson, 2009] is one minus the ratio of the empirical standard deviation of the EBEs, $SD(\hat{b})$, to the estimated random-effects standard deviation ω , where \hat{b} denotes the covariate-adjusted EBE. Large shrinkage values indicate weak individual information and reduce the reliability of EBE-based diagnostics. Values exceeding approximately 30% are commonly considered problematic [Savic and Karlsson, 2009].

2.7.3 Model comparison and cross-validation.

Competing model specifications are compared through their ability to predict unseen data. In mixed-effects models, predictive performance depends on whether predictions are made for previously observed individuals or for entirely new individuals, as discussed in Section 2.6. We therefore support both observation-level and subject-level cross-validation, which target these two prediction settings.

In subject-level cross-validation, entire individuals are assigned to held-out folds. Because no

observations from these individuals are available during training, predictions are generated as for unseen individuals, using either the plug-in predictor of Equation 48 or the marginal predictor of Equation 49. This setting evaluates the ability of the model to generalize to new individuals.

In observation-level cross-validation, only a subset of observations is held out for each individual. The remaining observations are used to estimate individual random effects, allowing predictions for the held-out observations to be generated as for known individuals, using either the EBE-based predictor of Equation 46 or the posterior average of Equation 47. This setting evaluates the ability of the model to predict additional observations from partially observed individuals.

Performance is assessed using the held-out predictive log-likelihood or a user-defined loss function.

2.8 Extension to Bayesian hierarchical models

The estimation and uncertainty quantification developed so far treat the population parameters θ as fixed unknowns and rely on large-sample approximations. The Bayesian formulation equips θ with a prior $p(\theta)$, and targets the posterior of population and random effects parameters jointly [Gelman et al., 2013].

2.8.1 Bayesian model framework.

The prior extends the two-level hierarchy of Equations 1 and 2 to a three-level hierarchy in which the prior generates the population parameters, the population parameters generate the random effects, and the random effects generate the observations [Wakefield, 1996, Lunn et al., 2002, Gelman et al., 1995, Davidian and Giltinan, 2003]. Inference targets the joint posterior of the population and random effects parameters,

$$p(\theta, \{B_i\} \mid \{(y_i, x_i)\}) \propto p(\theta) \prod_{i=1}^N p(B_i \mid x_i, \theta) p(y_i \mid x_i, B_i, \theta), \quad (15)$$

circumventing the need to estimate the integral in Equation 6, but replacing it with approximating a higher-dimensional posterior distribution, usually by MCMC. The Bayesian formulation does not remove the latent random effects from the model. Rather, it treats them as unknown quantities to be inferred jointly with the population-level parameters. In **NoLimits.jl**, the same model specification is reused for Bayesian inference: assigning priors to the population parameters switches estimation to MCMC sampling of the joint posterior of Equation 15 (Section 4).

A third route is variational inference, which approximates the posterior by the closest member of a tractable family of distributions, found by maximizing the ELBO [Blei et al., 2017].

2.8.2 Uncertainty quantification.

Posterior uncertainty is summarized directly from the MCMC draws that approximate the posterior of Equation 15. A credible interval for a component θ_k is reported as a pair of posterior quantiles, in contrast to the Wald and profile-likelihood intervals of Section 2.5, and propagates parameter uncertainty without the asymptotic-normality assumption [Gelfand and Smith, 1990].

3 Creating a NoLimits.jl model

A **NoLimits.jl** analysis is organized around a small set of macros and data structures rather than a fixed sequence of function calls. The workflow consists of four steps. First, a `Model` is defined using the `@Model` macro independently of any dataset. Second, the model is combined with a dataset to form a `DataModel`. Third, the model is fit with `fit_model`, producing a `FitResult` (Section 4). Finally, uncertainty quantification and model diagnostics are performed using `compute_uq` and the associated plotting utilities (Section 5).

The macro-based design provides the expressiveness of a high-level modeling language, while Julia’s multiple dispatch enables estimators, uncertainty-quantification methods, and model components to remain interchangeable and user-extensible. The remainder of this section introduces the `@Model` macro by constructing a model specification step by step, covering fixed effects, covariates, random effects, structural dynamics, and observation models.

3.1 The model macro

The first of the four steps, defining a `Model`, is carried out entirely with the `@Model` macro, which assembles the building blocks summarized in Table 1.

Each block is defined through a dedicated sub-macro, of which only `@fixedEffects` and `@formulas` are required. The blocks may be specified in any order and are sorted automatically during model construction.

As a minimal example, an exponential-decay model with a subject-specific decay rate can be written as follows.

```
model = @Model begin  
  @fixedEffects begin
```

```

    A      = RealNumber(10.0, scale = :log)
    k_pop  = RealNumber(0.0)
    omega  = RealNumber(0.3, scale = :log)
    sigma  = RealNumber(0.2, scale = :log)
end
@covariates begin
    t = Covariate()
end
@randomEffects begin
    k = RandomEffect(LogNormal(k_pop, omega); column = :id)
end
@formulas begin
    mu = A * exp(-k * t)
    y ~ Normal(mu, sigma)
end
end

```

While intentionally simple, this example illustrates the core structure of a model specification. In practice, the same blocks can express substantially richer models, while additional macros listed in Table 1 provide support for specialized components such as ODEs.

3.2 Fixed effects

The `@fixedEffects` block declares the population parameters and, where supported by the estimation method, the scale on which they are estimated. Each line defines a named parameter, whose identifier can subsequently be referenced throughout the model specification. To accommodate the diverse parameter types introduced in Section 2, **NoLimits.jl** provides parameter blocks ranging from unconstrained scalars to structured and constrained matrices. Table 2 summarizes the available parameter types and their associated reparameterizations.

3.2.1 Values, scales, bounds, and priors.

The scalar, vector, and matrix parameters (Table 2) are initialized from a starting value passed as the first positional argument, as in `RealNumber(0.0)`, with the remaining arguments optional keywords. The `scale` keyword selects the reparameterization from Table 2 and so determines the unconstrained coordinates used by the optimizer (Section 4): a positive parameter uses `scale = :log` and a probability `scale = :logit`, and a vector may carry a separate scale per element. The `lower` and `upper` keywords add box constraints for scalar and vector parameters. The `prior` keyword attaches a **Distributions.jl** distribution used

Block	Macro	Role	Required
Helpers	<code>@helpers</code>	Reusable sub-expressions shared across blocks	
Fixed effects	<code>@fixedEffects</code>	Population parameters with scales, bounds, and priors	✓
Covariates	<code>@covariates</code>	Time-varying, group-constant, and dynamic covariates	
Random effects	<code>@randomEffects</code>	Random effects and their distributions	
Pre-equation	<code>@preDifferentialEquation</code>	Quantities derived before solving the dynamics	
Dynamics	<code>@DifferentialEquation</code>	The system of ordinary differential equations	
Initial state	<code>@initialDE</code>	Initial conditions of the dynamics	
Observations	<code>@formulas</code>	Deterministic signals and the observation distribution	✓

Table 1: Building blocks of a `@Model` specification, in the canonical order in which the macro arranges them.

by the Bayesian estimators and ignored by the frequentist ones, and `calculate_se` controls whether a parameter enters the standard-error computation, defaulting to off for covariance matrices and differentiable machine-learning components.

3.2.2 Differentiable machine-learning components.

The differentiable machine-learning types of Table 2 are also declared in the `fixedEffects` but follow a different convention. Rather than a starting value and scale, each takes the structure that defines it, such as the network passed to `NNParameters`, together with a `function_name` used to call it from other blocks, and its coefficients are initialized internally. Section 3.8 outlines how they are embedded in a model.

3.3 Helpers

Model blocks frequently share the same algebraic expressions. The `@helpers` block defines small utility functions, such as link or saturation functions, that are reused across them. These functions could equally be defined in the surrounding Julia scope, but declar-

Type	Represents	Scales
<i>Scalar, vector, and matrix parameters</i>		
<code>RealNumber</code>	Scalar	<code>:identity</code> , <code>:log</code> , <code>:logit</code>
<code>RealVector</code>	Vector	<code>:identity</code> , <code>:log</code> , <code>:logit</code>
<code>RealDiagonalMatrix</code>	Diagonal matrix	<code>:log</code>
<code>RealPSDMatrix</code>	Covariance matrix	<code>:cholesky</code> , <code>:expm</code>
<code>ProbabilityVector</code>	Probability vector	<code>:stickbreak</code>
<code>DiscreteTransitionMatrix</code>	Transition matrix	<code>:stickbreakrows</code>
<code>ContinuousTransitionMatrix</code>	Rate matrix	<code>:lograterows</code>
<i>Differentiable machine-learning components</i>		
<code>NNParameters</code>	Neural network	–
<code>SoftTreeParameters</code>	Soft decision tree	–
<code>SplineParameters</code>	Spline basis	–
<code>NPFParameter</code>	Normalizing planar flow	–

Table 2: Fixed-effect parameter types, what each represents, and the reparameterizations available through the `scale` keyword. The scale defaults to the first one listed for each type, and the matrix, probability, and transition scales keep each parameter in its valid set, positive-definite, on the simplex, or row-stochastic. The differentiable machine-learning components take no `scale` argument and are estimated on an unconstrained basis.

ing them inside `@helpers` attaches them directly to the resulting `Model`, so that the model carries its own helpers and remains self-contained. Each entry is an ordinary function definition, for example `softplus(u) = log1p(exp(u))`, and is afterwards available by name in `@randomEffects`, `@preDifferentialEquation`, `@DifferentialEquation`, `@initialDE`, and `@formulas`. The block is optional and keeps repeated algebra in one place.

3.4 Covariates

Whereas fixed effects and helpers are internal to the model, covariates link it to the dataset. The `@covariates` block declares which columns are used by the model and how they are accessed during evaluation. Each covariate is assigned a name and a covariate type, for example `t = Covariate()`. The declared name is subsequently available throughout the model specification and is also used to retrieve values from the dataset. Consequently, each covariate name must correspond to a column in the data frame supplied when fitting the model.

NoLimits.jl distinguishes between three covariate types, each of which also has a vector-valued variant. The covariate type determines where in the model the covariate may be used

and how its values are accessed.

3.4.1 Covariate types.

1) A `Covariate()` is evaluated row by row and is therefore available only within the observation model specified in `@formulas`. 2) A `ConstantCovariate(; constant_on = :id)` is assumed constant within each individual and may be used throughout the model specification, allowing random-effects distributions, ODE initial conditions, ODE dynamics, and other model components to depend on observed covariates. 3) A `DynamicCovariate(; interpolation = LinearInterpolation)` is converted into a continuous function of time and can therefore be evaluated at arbitrary time points within the `@DifferentialEquation` block. For example, a dynamic covariate declared as `rate` is accessed as `rate(t)`. The interpolation method is selected from `DataInterpolations.jl` [Bhagavan et al., 2024], enabling piecewise-constant, linear, and nonlinear interpolation schemes.

Each covariate type also has a vector-valued counterpart (`CovariateVector` and its constant and dynamic variants), which groups multiple columns under a single name. The grouped name then behaves directly as a numeric vector, so it can be passed as a whole wherever a vector is expected, while the individual columns remain accessible by name. This is particularly useful when covariates are used collectively, for example as inputs to a neural network, as in `NN(x, nn)`.

3.5 Random effects

The `@randomEffects` block defines the between-subject variability of the model through the random effects B_i introduced in Section 2. Each random effect is associated with a grouping variable and is shared by all observations within the same group. As with covariates, the grouping variable must correspond to a column in the dataset supplied during model fitting.

3.5.1 Declaring random effects.

A random effect is declared as `eta = RandomEffect(dist; column = ...)`, where `eta` is the name of the random effect, `dist` specifies its distribution, and `column` identifies the grouping variable. Distribution parameters may depend on fixed effects and constant covariates, allowing covariate-dependent random-effects distributions. Multiple random effects can be defined on the same or different grouping variables, supporting nested and crossed random-effects structures (Appendix A.1).

Once declared, a random effect can be referenced by name in all model blocks listed in Table 1, except `@fixedEffects`.

3.5.2 Flexible random-effects distributions.

Random effects can be modeled using arbitrary continuous distributions with finite mean from **Distributions.jl**, including heavy-tailed, skewed, strictly positive, and multivariate distributions such as `MvNormal`. Components of multivariate random effects can be accessed by indexing, for example `eta[1]`.

When a modeler aims for a nonparametric random effects distribution, the random-effects distribution can instead be learned from the data using a normalizing planar flow. For example, a flow parameter declared among the fixed effects as `psi = NPFParameter(2, 2)` defines a random effect through `RandomEffect(NormalizingPlanarFlow(psi); column = :id)`. The flow parameters are estimated jointly with the remaining model parameters, enabling flexible multivariate distributions that can capture skewness and multimodality through **NormalizingFlows.jl**.

3.6 Structural dynamics

The blocks introduced so far describe quantities evaluated directly from parameters and covariates. Mechanistic models additionally evolve internal states over time, specified through up to three ODE blocks: one for quantities computed before integration, one for the system dynamics, and one for the initial conditions. All three blocks have access to fixed effects, random effects, constant covariates, and arbitrary transformations thereof, while the `@DifferentialEquation` block may additionally access dynamic covariates.

The following example illustrates the basic structure,

```
@covariates begin
    dose = ConstantCovariate()
end
@preDifferentialEquation begin
    k = exp(log_k + eta_k)
end
@DifferentialEquation begin
    D(A) ~ -k * A
    flux(t) = k * A
end
@initialDE begin
    A = dose
end
```

which we further explain below.

3.6.1 Pre-integration computations.

The optional `@preDifferentialEquation` block is used for calculations that do not depend on the state trajectory and therefore need only be performed once per individual. Typical examples include transforming fixed and random effects into individual parameters, as in $k = \exp(\log_k + \text{eta_k})$. Although such expressions could be placed directly in the differential equations, evaluating them before integration avoids unnecessary computations during solver execution.

3.6.2 Dynamical system.

The `@DifferentialEquation` block defines the system dynamics through equations of the form $D(\text{state}) \sim \text{rhs}$. It may additionally define named signals such as $\text{flux}(t) = k * A$, representing derived quantities that depend on time and the current state. Both states and signals are available to the observation model and may be referenced elsewhere in the model specification.

The resulting system is solved using `OrdinaryDiffEq.jl`, and the solution is exposed as a continuous function of time.

3.6.3 Accessing states and signals.

States and signals can be accessed in the `@formulas` block as $A(t)$ and $\text{flux}(t)$. Because the solution is continuous in time, they may also be evaluated at shifted time points, such as $A(t - 0.5)$, enabling the representation of delays and carry-over effects.

3.6.4 Initial conditions.

Initial conditions are specified in the `@initialDE` block. In the example above, the initial state depends on the covariate `dose`. More generally, initial conditions may depend on fixed effects, random effects, covariates, or learned model components.

3.7 Observation models

The `@formulas` block is where states, fixed and random effects, and covariates are linked to the conditional observation models (Equation 2). It is the most flexible block in the model definition and has access to all previously defined quantities.

We use the following example to illustrate its capabilities.

```

@formulas begin
  conc = A(t) / V
  c ~ Normal(conc, sqrt(sigma_add^2 + (sigma_prop * conc)^2))
  count ~ Poisson(exp(eta + beta * t))
end

```

The block distinguishes between two types of specifications. The first defines a deterministic signal, such as `conc = A(t) / V`, using an equality sign. The second defines a distributional relationship, such as `c ~ Normal(conc, sqrt(sigma_add^2 + (sigma_prop * conc)^2))`, using the `~` operator.

3.7.1 Deterministic signals.

A deterministic line of the form `name = term` introduces a named signal. This signal can be further processed within the `@formulas` block or passed to a distributional relationship to parameterize a conditional observation distribution. For example, `conc = A(t) / V` defines the signal `conc`, which is subsequently used in the observation model.

The defining expression can be nearly arbitrarily complex and may involve any previously defined quantities, including states, parameters, fixed and random effects, and covariates.

3.7.2 Distributional relationships.

A line of the form `name_y ~ dist` links an observed variable to a conditional probability distribution, as in `name_y ~ Poisson(exp(eta + beta * t))`. The variable `name_y` must correspond to a column in the observation data and is automatically associated with the specified conditional distribution.

Any univariate distribution from **Distributions.jl** that admits a finite density under the chosen parameterization can be used. As a result, continuous, count, binary, and other observation types are specified uniformly. Vector-valued distributions can additionally be used to model correlation within the conditional observation model.

Because the parameters of a distribution are themselves arbitrary expressions, complex dependencies between the conditional observation distribution and other model quantities can be specified directly.

For example, a constant standard deviation, `c ~ Normal(conc, sigma)`, defines an additive error model, whereas a standard deviation proportional to the prediction, `c ~ Normal(conc, sigma_prop * conc)`, defines a proportional error model. Combining additive and proportional terms yields a combined additive-and-proportional error model.

3.7.3 Multiple observations.

Multiple observation models can be specified within the same `@formulas` block when multiple observed variables are available. In the example above, `c` is a continuous variable and `count` is a count variable. Consequently, each individual contributes observations from two different distribution families (Appendix A.2).

3.7.4 Censored observations.

Censored observations, whose values are only known to lie within an interval (for example, below a lower limit of quantification), are supported through the **Distributions.jl** interface. One wraps the observation distribution as

```
c ~ censored(Normal(conc, sigma), lower = lloq, upper = Inf),
```

where either bound may be specified as a constant value shared across all observations or as a covariate column, allowing observation-specific censoring limits (Appendix A.3). Combining a survival-time observation distribution such as `Exponential` or `Weibull` with right-censoring in this way expresses parametric time-to-event models, which therefore require no dedicated machinery beyond the general observation-model and censoring interface.

3.7.5 Markov observation models.

In **NoLimits.jl**, Markov models are implemented as observation distributions and are therefore specified in the same way as any other stochastic model component. **NoLimits.jl** provides hidden- and observed-state models in discrete- and continuous-time variants, with univariate emissions, multivariate emissions with missing observations, and coarsened observed states (Table S1). All components of these models can be defined as arbitrary expressions and may therefore depend on covariates, fixed and random effects, or learned components such as neural networks. A worked HMM specification, together with the forward recursion that defines its conditional likelihood, is given in Appendix A.4.

3.8 Embedding differentiable machine-learning components

A distinguishing feature of **NoLimits.jl** is that differentiable machine learning components are treated as ordinary parameter blocks and can be used throughout a model. The available component types are listed in Table 2. Each component is declared in `@fixedEffects` via `params = NNParameters(args; function_name = :func_name)`, where the function name is mandatory. The component can then be called from any other block as `func_name(inputs, params)`, passing the input vector and the parameter block.

Neural networks and soft decision trees return vectors and therefore require indexing to select a particular output component, for example `func_name(inputs, params)[j]`. In contrast, splines map a scalar input to a scalar output and can be used directly without indexing. The example below declares one component of each type and uses the neural network in the random-effect distribution, the soft tree in the system dynamics, and the spline in the observation model. The model serves only to illustrate the flexibility with which machine-learning components can be integrated into **NoLimits.jl** models.

```

using SimpleChains
chain = SimpleChain(static(2), TurboDense(tanh, 4), TurboDense(identity, 1))

@fixedEffects begin
    theta      = RealVector([0.5, 1.0, 0.3, 0.2], scale = fill(:log, 4))
    par_nn     = NNParameters(chain; function_name = :NN)
    par_st     = SoftTreeParameters(2, 3; function_name = :ST)
    par_sp     = SplineParameters(0.0:1.0:10.0; function_name = :SP)
end

@covariates begin
    x = ConstantCovariateVector([:age, :bmi]; constant_on = :id)
end

@randomEffects begin
    eta = RandomEffect(
        Normal(NN(x, par_nn)[1], theta[3]); column = :id
    )
end

@DifferentialEquation begin
    D(A) ~ ST([A, t], par_st)[1] - theta[1] * A
end

@formulas begin
    conc = A / theta[2]
    y ~ Normal(SP(conc, par_sp) + eta, theta[4])
end

```

In `@randomEffects`, the network `NN` maps the subject-level covariates `age` and `bmi` to the mean of the random effect distribution. Because random effects are defined once per subject, their inputs must be constant within a subject. In `@DifferentialEquation`, the soft tree `ST` adds a learned state- and time-dependent term to the dynamics of `A`, turning the system into a universal differential equation (UDE). Finally, in `@formulas`, the spline `SP` maps the deterministic signal `conc` to the conditional observation mean, with its coefficients estimated as fixed effects on the knot vector specified in `SplineParameters`.

Because machine-learning components are ordinary parameter blocks, new component types can be integrated by defining their parameter type and evaluation function, without modifying the rest of the framework.

The network passed to `NNParameters` is a **SimpleChains.jl** `SimpleChain` with two inputs, a hidden layer of four `tanh` units, and a linear output layer. The same code would also work with a **Lux.jl** `Chain`, with only the network object changing. The call convention, estimators, and optimization routines remain unchanged. We generally recommend **SimpleChains.jl** for the small CPU-resident networks commonly used in NLME models because it is faster and more memory efficient, while **Lux.jl** is preferable when more expressive architectures are required.

3.9 Binding a model to data

A `Model` is independent of any particular dataset and is bound to one with the `DataModel` constructor.

3.9.1 Data format.

The data are supplied as an ordinary **DataFrames.jl** [Bouchet-Valat and Kamiński, 2023] data frame in long format, passed as `df` in `DataModel(model, df; primary_id = :id, time_col = :t)`, with `primary_id` the subject identifier and `time_col` the time column. The data frame stacks the records of all subjects on top of one another, one row per record, the layout used by **NONMEM** and **Monolix**. Each row carries the subject identifier, the time, the observations named on the stochastic lines of `@formulas`, the covariates named in `@covariates`, and the grouping columns named in `@randomEffects`. An observation that is not measured in a given row is left `missing`, so a row that records only a dose or a covariate value carries `missing` in its observation columns.

3.9.2 Dosing and events.

For ODE-based models, doses and other interventions are specified through event records in the data, following the conventions of **NONMEM** and **Monolix**. Event handling is enabled by passing an event column to the data model `DataModel` construction,

```
dm = DataModel(model, df;  
  primary_id = :id,  
  time_col = :t,  
  evid_col = :EVID)
```

Column	Keyword	Role
EVID	<code>evid_col</code>	Event type, with 0 an observation, 1 a dose, and 2 a compartment reset
AMT	<code>amt_col</code>	Dose amount, or the value a compartment is set to on a reset
RATE	<code>rate_col</code>	Infusion rate, with 0 a bolus and for a positive value an infusion
CMT	<code>cmt_col</code>	Target compartment, given as a state name

Table 3: Event columns of the long data table, read when `evid_col` is set. The keyword column gives the `DataModel` argument that names each column, and the amount, rate, and compartment keywords default to `:AMT`, `:RATE`, and `:CMT`.

Rows with `EVID = 0, 1, and 2` denote observations, doses, and compartment resets, respectively. Doses may be administered as boluses or infusions, and target compartments are specified through `CMT` (Table 3).

3.9.3 Construction and validation.

Constructing the `DataModel` checks that the required columns are present, partitions the rows by the primary identifier into one `Individual` per subject, and precomputes the grouping structure used by the random-effect blocks. The resulting `DataModel` is the object passed to every estimator in the next section.

4 Parameter estimation in `NoLimits.jl`

All estimation methods in `NoLimits.jl` share a common interface. Each estimator is represented by a Julia struct, and a model is fit by passing a `DataModel` together with the desired estimator to `fit_model`. Consequently, switching between estimation methods requires changing only the estimator struct, while the model specification and data binding remain unchanged. Estimation with the Laplace method only requires only minimal code.

```
res_lap = fit_model(dm, Laplace())
```

Other estimators can be used by replacing `Laplace()`, with the corresponding estimator constructor. Table 4 summarizes the available estimators, the inference paradigms they implement, their support for random effects, and their typical use cases. Together, they cover the methods described in Sections 2.4 and 2.8. If an estimator is incompatible with the specified model, for example because a fixed-effects-only method is applied to a mixed-effects model or a Bayesian estimator is used without prior distributions, `NoLimits.jl` produces an informative error message. Variational inference is currently available for fixed-effects-only

Estimator	Inference	Random or Fixed	Typical use
MLE	Likelihood	Fixed	Models without random effects
MAP	Posterior	Fixed	Fixed effects with priors
Pooled	Likelihood	Fixed	Starting values for mixed-effects fits
PooledMap	Posterior	Fixed	Starting values for mixed-effects fits with priors
Laplace	Approximate likelihood	Random	Small number of random effects
FOCEI	Approximate likelihood	Random	Moderate number of random effects
MCEM	Stochastic EM	Random	When the Laplace approximation is inadequate
SAEM	Stochastic EM	Random	Moderate number of random effects and/or non-Gaussian posterior
MCMC	Bayesian sampling	Both	Full posterior inference
VI	Approximate Bayesian	Fixed	Fast approximate posterior

Table 4: Estimators available through `fit_model`, the inference paradigm each implements, whether it accommodates random effects, and the setting in which each is typically used.

models through the VI estimator, with variational inference over the random effects planned as a future extension.

All estimation methods share the numerical optimization, parameter transformation, and multistart machinery described in the remainder of this section. Mixed-effects models can additionally be warm-started from a pooled fit that ignores the random-effect structure by passing `pooled_init = true` to `fit_model`.

4.1 Numerical optimization and parameter transformations

The estimators in **NoLimits.jl** share a set of numerical components that are configured separately from the model and its data binding. Each can be swapped or returned on its own, leaving the model specification and the remaining components untouched.

4.1.1 Numerical optimization.

Whenever numerical optimization is required, **NoLimits.jl** interfaces with **Optimization.jl**, providing access to a broad range of gradient-based and gradient-free optimization algorithms

from packages such as **Optim.jl** [Mogensen and Riseth, 2018], **NLopt.jl** [Johnson, 2007] and **BlackBoxOptim.jl** [Feldt and Stukalov, 2026]. The default optimizer for the Laplace and FOCEI outer optimization is the gradient-free BOBYQA [Powell et al., 2009] algorithm implemented in NLopt.jl. For all other numerical optimization tasks, the default is the limited-memory Broyden-Fletcher-Goldfarb-Shanno (L-BFGS) algorithm [Liu and Nocedal, 1989] and gradients are computed via forward-mode automatic differentiation using **Forward-Diff.jl**. Every estimator that performs numerical optimization exposes the same two controls, the `optimizer` object and the `optim_kwarg`s named tuple, the latter forwarded verbatim to `Optimization.solve` so that iteration caps and solver tolerances are set without leaving the estimator constructor. Selecting a different algorithm is a one-line change that leaves the model and data specification untouched. For example,

```
res = fit_model(dm, Laplace(optimizer = NoLimits.LBFGS(),
                             optim_kwarg = (maxiters = 200,)))
```

will use the L-BFGS implementation from **Optim.jl** for the outer optimization of the Laplace algorithm. The automatic differentiation backend is currently fixed to forward mode.

4.1.2 Parameter transformations.

Parameter transformations are defined by the `scale` keyword argument when defining fixed effects (Table 2). The scale transforms a constrained parameter, e.g., a positive real number, to an unconstrained parameter allowing the optimizer to operate in an unconstrained space. The inverse map recovers the natural values for likelihood evaluation. More complex examples include parameterizations of variance covariance matrices, which must be positive definite. This is achieved in **NoLimits.jl** by estimating the Cholesky factorization (`scale = :cholesky`) or its matrix logarithm and matrix exponential (`scale = :expm`). Domains are therefore enforced by construction rather than through box constraints or penalty terms, so the optimization stays unconstrained even when the parameters are bounded, positive-definite, or confined to a simplex. This is in contrast to specifying box-constraints via `lower` and `upper`, which uses constrained optimization.

For Bayesian estimation, priors are specified on the untransformed parameter scale. Consequently, Bayesian methods do not use the parameter transformations or box constraints specified for frequentist estimation. Parameter values outside the admissible domain of the prior are instead assigned an objective value of $-\infty$.

Two further numerical components are configured in the same separable way, the **Multistart** procedure that guards against local optima and the ODE solver selected. Both are described in Appendix A.10.

5 Uncertainty quantification and visualization in **NoLimits.jl**

Uncertainty quantification in **NoLimits.jl** is performed through the single function `compute_uq`, which takes a `FitResult` and returns a `UQResult`. Depending on the chosen method, the result contains point estimates together with confidence or credible intervals and, where available, the covariance matrix and the underlying parameter draws. All quantities are reported on both the natural and transformed parameter scales.

The uncertainty construction is selected through the `method` keyword and its coverage through `level`. By default, **NoLimits.jl** chooses a method consistent with the estimator used for fitting, for example Wald intervals for frequentist estimators and posterior intervals for Bayesian estimators. These constructions correspond to the methods described in Section 2.5.

A `UQResult` can be inspected with `summarize(uq)` and further visualized with the provided function `plot_uq_distributions`. The remainder of this section introduces the plotting functions used to assess fitted models, their predictions, and the associated uncertainty.

5.1 Wald and sandwich intervals

With `method = :wald`, confidence intervals are computed from the inverse observed information matrix, while `method = :sandwich` uses the robust sandwich covariance estimator (Section 2.5).

```
uq = compute_uq(res; method = :wald, level = 0.95)
```

These methods are computationally inexpensive and therefore the default for likelihood-based estimators. Their validity relies on large-sample asymptotics and, in practice, on the objective function being approximately quadratic in a neighborhood of the optimum.

5.2 Profile-likelihood intervals

With `method = :profile`, **NoLimits.jl** computes profile-likelihood intervals through **LikelihoodProfiler.jl** [Borisov et al., 2026].

```
uq = compute_uq(res; method = :profile)
```

Unlike Wald intervals, these do not rely on a local quadratic approximation of the log-likelihood and are therefore more reliable for asymmetric or weakly identifiable parameters, at the cost of potentially costly repeated model refits (Section 2.5).

5.3 Posterior intervals

With `method = :chain`, uncertainty intervals are obtained from quantiles of posterior samples,

```
uq = compute_uq(res; method = :chain)
```

For an MCMC fit, the posterior samples are already available. For likelihood-based fits, **NoLimits.jl** can optionally refit the model using MCMC and compute intervals from the resulting posterior draws. These intervals do not rely on asymptotic approximations and correspond to Bayesian credible intervals (Section 2.8). Users should be aware that, in the latter case, uncertainty quantification is based on a Bayesian rather than a frequentist interpretation of probability.

5.4 Unified plotting style

NoLimits.jl provides a family of plotting functions, built on **Plots.jl** [Breloff et al., 2026], that act on a `FitResult`, or, for parameter uncertainty, on a `UQResult`. They share a common `PlotStyle` options object, so a consistent appearance is applied across an analysis by constructing one `PlotStyle` and passing it to each call through the `style` keyword.

```
ps = PlotStyle()  
plot_vpc(res; style = ps)  
plot_residual_qq(res; style = ps)
```

Each function returns a **Plots.jl** object that is displayed, saved, or composed like any other plot.

6 Examples

We illustrate the main functionality of **NoLimits.jl** through three case studies that span different model classes supported by the package: a compartmental ODE model for warfarin pharmacokinetics (Section 6.1), a learnable concentration-effect function embedded in the pharmacodynamic dynamics of the same drug (Section 6.2), and a normalizing flow as a flexible random-effects distribution (Section 6.3). Further supported model classes, including the discrete- and continuous-time Markov models described in Section 3 and Appendix A.4, are documented in the software sections rather than exercised in a worked example here. All scripts and figure-rendering code are provided in the replication code. The code blocks below

show only the **NoLimits.jl** API calls that constitute the core analysis workflow. We use a common `PlotStyle` type for all **NoLimits.jl** plotting functions for a unified plot styling. All figures across the three case studies share a single instance:

```
my_style = PlotStyle(  
    base_subplot_width = 500,  
    base_subplot_height = 400,  
    font_size_title = 18,  
    font_size_label = 15,  
    font_size_tick = 14,  
    font_size_legend = 14,  
    font_size_annotation = 12,  
)
```

6.1 Warfarin pharmacokinetics: a one-compartment ODE model

Warfarin is an anticoagulant typically used to treat blood clots. It can exhibit substantial inter-individual variability in exposure, making it a standard benchmark for population pharmacokinetic modeling [Lane et al., 2012]. A common approach is a compartmental ODE embedded in an NLME model with random effects and weight-based covariates. **NoLimits.jl** provides a composable implementation of this model class with interchangeable estimators and built-in diagnostics. We fit a warfarin model using MCEM, quantify uncertainty, assess fit, characterize inter-individual variability, and then refit the same model by MCMC to obtain a full Bayesian posterior.

6.1.1 Data

We use the warfarin pharmacokinetics dataset from the **Monolix** tutorial library [Simulations Plus, 2024]. It contains repeated plasma concentration measurements for 32 healthy volunteers following a single oral dose. The dataset is loaded with `load_warfarin_from_monolix()`, which downloads the data and converts them directly to the **NoLimits.jl** format. In the analysis below, we use the subject identifier (`id`), observation time (`t`), dose (`d`), body weight (`wt`), and plasma concentration (`C`).

```
df = NoLimits.load_warfarin_from_monolix()  
first(select(df, :id, :t, :d, :wt, :C), 5)
```

5x5 DataFrame

Row	id	t	d	wt	C
-----	----	---	---	----	---

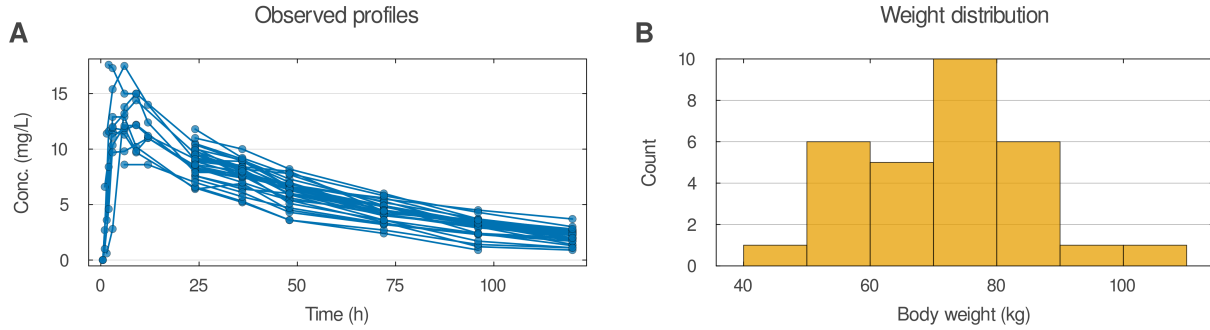


Figure 2: (A) Observed plasma warfarin concentrations versus time for 32 subjects. Each line represents one subject. Produced with the **NoLimits.jl** function `plot_observed_profiles`. (B) Body weight distribution across subjects.

	String	Float64	Float64	Float64	Float64?
1	1	0.0	100.0	66.7	missing
2	1	24.0	100.0	66.7	9.2
3	1	36.0	100.0	66.7	8.5
4	1	48.0	100.0	66.7	6.4
5	1	72.0	100.0	66.7	4.8

The first five rows show that the dose `d` and the weight `wt` are constant within a subject, while time `t` and concentration `C` vary across measurement occasions. The plasma concentration profiles exhibit the characteristic absorption peak followed by log-linear elimination, with substantial inter-individual variability in both peak concentration and elimination rate (Figure 2A). Body weight ranges from 40 to 102 kg (Figure 2B).

6.1.2 Model specification

We specify a one-compartment first-order absorption pharmacokinetic model to describe the warfarin plasma concentration-time profiles. For subject i receiving dose d_i , the depot amount $A_{\text{dep},i}(t)$ and central-compartment amount $A_{\text{cen},i}(t)$ evolve according to the ODE system

$$\frac{dA_{\text{dep},i}}{dt} = -k_{a,i} A_{\text{dep},i}(t), \quad \frac{dA_{\text{cen},i}}{dt} = k_{a,i} A_{\text{dep},i}(t) - \frac{\text{CL}_i}{V_i} A_{\text{cen},i}(t). \quad (16)$$

with initial conditions $A_{\text{dep},i}(0) = d_i$ and $A_{\text{cen},i}(0) = 0$. Here $k_{a,i}$ (h^{-1}) is the first-order absorption rate, CL_i (L/h) is the apparent clearance, and V_i (L) is the apparent volume of distribution. All three are assumed to follow a log-normal random effect structure to enforce

their positivity:

$$\begin{aligned}
k_{a,i} &\sim \text{LogNormal}(\mu_{k_a}, \sigma_{k_a}^2), \\
\text{CL}_i &\sim \text{LogNormal}\left(\mu_{\text{CL}} + 0.75 \log\left(\frac{w_i}{70}\right), \sigma_{\text{CL}}^2\right), \\
V_i &\sim \text{LogNormal}(\mu_V, \sigma_V^2),
\end{aligned}
\tag{17}$$

where w_i is the body weight of subject i (kg) and 70 kg is chosen as the reference weight. The allometric exponent of 0.75 follows established pharmacometric practice [Wang et al., 2012]. Observed plasma concentrations C_{ij} at time t_{ij} are linked to the ODE solution by

$$C_{ij} \mid k_{a,i}, \text{CL}_i, V_i \sim \mathcal{N}\left(\frac{A_{\text{cen},i}(t_{ij})}{V_i}, \sigma_C^2\right),
\tag{18}$$

The depot and central compartments of Equation 16 form a linear system whose central-compartment amount has the closed-form Bateman solution

$$A_{\text{cen},i}(t) = d_i \frac{k_{a,i}}{k_{a,i} - k_{e,i}} \left(e^{-k_{e,i} t} - e^{-k_{a,i} t} \right), \quad k_{e,i} = \frac{\text{CL}_i}{V_i},
\tag{19}$$

which we evaluate directly in place of numerical integration. This yields seven estimable parameters: the population log-means μ_{k_a} , μ_{CL} , μ_V , the random-effect standard deviations σ_{k_a} , σ_{CL} , σ_V , and the residual error σ_C . Each population parameter additionally carries a uniform prior, which bounds it for frequentist estimation and serves as its prior for Bayesian estimation, so a single specification supports both. The `@Model` macro encodes the closed-form solution (Equation 19), the random-effect structure (Equation 17), and the observation model (Equation 18) through a helper function:

```

model = @Model begin
  @helpers begin
    bateman_center(t, dose, ka, ke) = abs(ka - ke) < 1e-8 ?
      dose * ka * t * exp(-ka * t) :
      dose * ka / (ka - ke) * (exp(-ke * t) - exp(-ka * t))
  end
  @fixedEffects begin
    ka_mean      = RealNumber(0.0,  prior = Uniform(-2, 2))
    CL_mean      = RealNumber(-0.5, prior = Uniform(-3, 3))
    V_mean       = RealNumber(4.0,  prior = Uniform(1, 4))
    sigma_ka     = RealNumber(2.0,  scale = :log, prior = Uniform(0, 4))
    sigma_CL     = RealNumber(2.0,  scale = :log, prior = Uniform(0, 4))
    sigma_V      = RealNumber(2.0,  scale = :log, prior = Uniform(0, 4))
    sigma_C_error = RealNumber(2.0,  scale = :log, prior = Uniform(0, 4))
  end
end

```

```

@covariates begin
  t = Covariate()
  d = ConstantCovariate(; constant_on = :id)
  wt = ConstantCovariate(; constant_on = :id)
end
@randomEffects begin
  ka = RandomEffect(LogNormal(ka_mean, sigma_ka); column = :id)
  CL = RandomEffect(
    LogNormal(CL_mean + 0.75 * log(wt / 70.0), sigma_CL);
    column = :id)
  V = RandomEffect(LogNormal(V_mean, sigma_V); column = :id)
end
@formulas begin
  C ~ Normal(bateman_center(t, d, ka, CL / V) / V, sigma_C_error)
end
end

dm = DataModel(model, df; primary_id = :id, time_col = :t)

```

The `bateman_center` helper implements the closed-form solution of Equation 19. The four standard deviations are estimated on the log scale (`scale = :log`), which enforces positivity by construction. After the model definition, `DataModel(model, df; primary_id = :id, time_col = :t)` attaches the model to the data.

6.1.3 Estimation and uncertainty quantification

Parameter estimation uses MCEM with `store_diagnostics = true` to record per-iteration parameter trajectories and Wald-type 95% confidence intervals are obtained from the observed Fisher information matrix at the MCEM estimate:

```

Random.seed!(12243)
fit = fit_model(dm, MCEM(maxiters = 60, store_diagnostics = true))
uq = compute_uq(fit)
summarize(uq)

```

UQResultSummary

=====

Overview

backend : wald

```

source_method          : mcem
inference              : frequentist
scale                  : natural
interval level        : 0.95
parameters shown (reported / total) : 7 / 7

```

Parameter uncertainty summary

parameter	Estimate	Std. Error	CI Lower	CI Upper
ka_mean	-0.5097	0.1943	-0.8859	-0.1144
CL_mean	-2.0484	0.038	-2.1259	-1.9761
V_mean	2.0526	0.0475	1.9585	2.1456
sigma_ka	0.6445	0.0269	0.5933	0.7009
sigma_CL	0.1706	0.0342	0.1163	0.2495
sigma_V	0.2205	0.0382	0.1583	0.3021
sigma_C_error	1.0499	0.0577	0.9403	1.1731

The population estimates correspond to a median absorption rate of approximately 0.60 h^{-1} , a median clearance of 0.13 L/h at the 70 kg reference weight, and a median volume of distribution of 7.8 L . The confidence intervals for clearance and volume are relatively narrow, indicating good identifiability, whereas the wider interval for the absorption rate reflects the limited information available during the early absorption phase. These are frequentist point estimates with Wald-type intervals. Because the estimator is selected by a single argument to `fit_model`, the same model is also fit by MCMC to obtain a full Bayesian posterior, which we examine in Section 6.1.5.

6.1.4 Results and diagnostics

Individual and population calibration are assessed jointly in Figure 3. The individual fit is examined first, for three randomly selected subjects:

```

fig3_idx = sort(randperm(MersenneTwister(42), 32)[1:3])
fig3 = plot_fits(fit; individuals_idx = fig3_idx, ncols = 3, style = my_style,
                kwargs_subplot = (xlabel = "Time (h)", ylabel = "Concentration (mg/L)"))

```

Population-level calibration is then assessed with a VPC and two goodness-of-fit comparisons of predictions, residuals, and observed values:

```

p_vpc = plot_vpc(fit; n_simulations = 1000, percentiles = [5, 50, 95],
                 style = my_style)

```

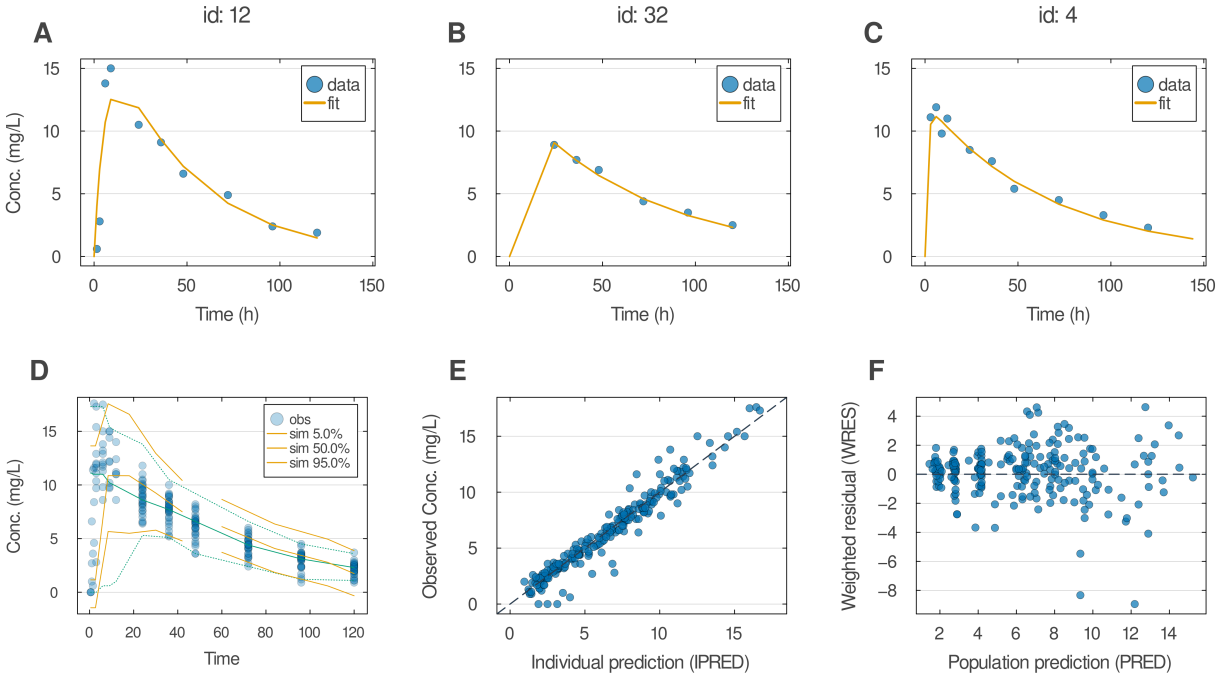


Figure 3: Model fit diagnostics for the warfarin analysis. (A)–(C) Posterior predictions (curves) overlaid on observed plasma concentrations (dots) for three randomly selected subjects (top row), produced with `plot_fits`. (D) Visual predictive check with 5th, 50th, and 95th simulated percentile envelopes (shaded bands) and observed sample quantiles (solid lines) based on 1000 simulations, produced with `plot_vpc`. (E) Observed concentration against IPRED evaluated at EBEs, produced with `plot_dv_ipred`. (F) WRES against PRED, produced with `plot_wres_pred`.

```
p_ipred = plot_dv_ipred(fit; style = my_style)
p_wres  = plot_wres_pred(fit; style = my_style)
```

The fitted model captures the absorption peak and the subsequent log-linear elimination for all three subjects (Figure 3A–C), and the between-subject differences in peak height and elimination slope reflect the estimated inter-individual variability in ka , CL , and V . The VPC (Figure 3D) confirms that the population model reproduces the marginal variability of the data across the full time course. Predictions evaluated at the EBEs agree closely with the observed concentrations (Figure 3E). The WRESs are approximately symmetric about zero with no systematic trend against the PRED (Figure 3F), indicating that the additive residual error model is appropriate for this dataset.

The MCEM convergence trajectories and the inter-individual variability of the three random effects, including the empirical-Bayes shrinkage and the body-weight dependence of clearance, are reported in Appendix B.1.

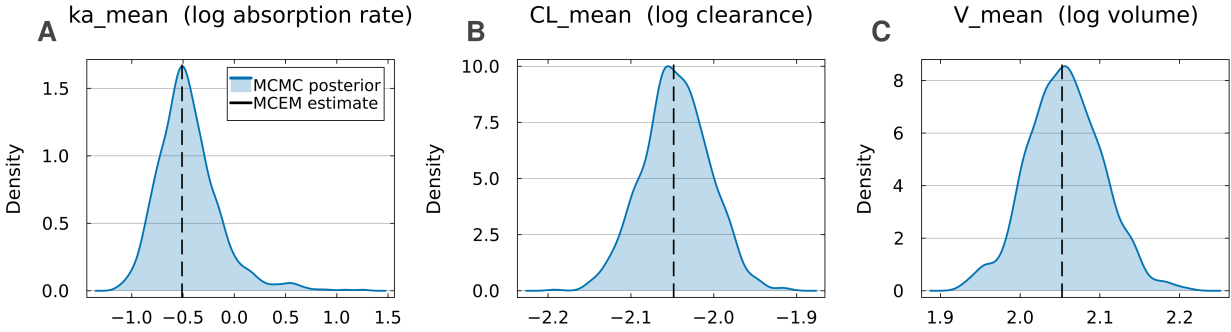


Figure 4: Marginal posterior distributions of the population log-means from the Bayesian fit (MCMC with the NUTS), with the corresponding MCEM point estimates as dashed lines: (A) μ_{k_a} , (B) μ_{CL} , (C) μ_V .

6.1.5 Bayesian analysis

The model defined above already declares a uniform prior on every population parameter, so a full Bayesian analysis needs no change to the specification, only a different estimator. We draw from the posterior with the NUTS [Hoffman et al., 2014] through the **Turing.jl** backend [Ge et al., 2018, Fjelde et al., 2025], and the closed-form solution (Equation 19) keeps the sampling inexpensive:

```
fit_mcmc = fit_model(dm, MCMC(); rng = MersenneTwister(3))
```

Figure 4 compares the marginal posteriors of the population log-means with the corresponding MCEM estimates. The posterior modes closely match the MCEM point estimates, indicating good agreement between the frequentist and Bayesian analyses. Clearance and volume are well identified, with narrow, approximately symmetric posteriors. In contrast, the absorption-rate posterior is broader and right-skewed, reflecting the limited information available on the absorption phase. This asymmetry is captured by the posterior distribution but not by a point estimate or the symmetric Wald interval from the MCEM estimation. Posterior summaries for the random-effect and outcome distribution standard deviations are reported in Appendix B.1.3.

6.2 Warfarin pharmacodynamics: a learnable concentration-effect function

The one-compartment model of Section 6.1 captures warfarin plasma concentrations well, but the same dataset also contains international normalized ratio (INR) measurements, which we

have ignored in the previous model. A standard pharmacodynamic (PD) model links concentration to an indirect-response turnover model through a saturable **E_{max}** effect [Dayneka et al., 1993]. Alternatively, this relationship can be learned directly from the data. **NoLimits.jl** supports this by allowing users to embed differentiable machine-learning components directly into the turnover model. We demonstrate this with neural-network and soft-tree models and use cross-validation (CV) to compare them against the parametric model, showing how a learned effect function serves as a diagnostic for the assumed concentration-effect shape even when predictive performance is unchanged.

6.2.1 Learnable concentration-effect dynamics

This PD model extends the pharmacokinetic (PK) model of Section 6.1. The depot and central compartments of Equation 16 are kept unchanged, and an indirect-response turnover compartment is added on top, driven by the plasma concentration $C_i(t) = A_{\text{cen},i}(t)/V_i$ from that submodel. Writing R_i for the response of subject i , $R_{0,i}$ for its baseline, and $k_{\text{out},i}$ for the turnover rate, the drug modifies the loss of the response through

$$\frac{dR_i}{dt} = k_{\text{out},i} \left(R_{0,i} - R_i(t) \left(1 + \mathcal{E}(C_i(t)) \right) \right), \quad R_i(0) = R_{0,i}, \quad (20)$$

where \mathcal{E} is a concentration-effect function. For this concentration-effect function, we compare a parametric saturable effect with a learnable one,

$$\mathcal{E}(C) = \frac{E_{\text{max}} C}{\text{EC}_{50} + C} \quad \text{or} \quad \mathcal{E}(C) = C \zeta(\text{ML}(C/c_0)), \quad (21)$$

where ML is a neural network or a soft decision tree, ζ the softplus function ensuring a nonnegative effect, c_0 a fixed concentration scale, and the leading factor C ensures no effect at zero concentration. For conciseness in the main manuscript, the full `@Model` specification of the parametric **E_{max}** model is given in Appendix B.2. The neural network-based model embeds a small **SimpleChains.jl** network in the response dynamics:

```
chainE = SimpleChain(static(1), TurboDense(tanh, 4), TurboDense(identity, 1))

model_nn = @Model begin
    @helpers begin
        softplus(u) = u > 20 ? u : log1p(exp(u))
    end
    @fixedEffects begin
        ka_mean      = RealNumber(0.0); CL_mean      = RealNumber(-2.0)
        V_mean       = RealNumber(2.0); kout_mean    = RealNumber(-3.0)
        sigma_ka     = RealNumber(0.3, scale = :log)
    end
end
```

```

    sigma_CL = RealNumber(0.3, scale = :log)
    sigma_V  = RealNumber(0.3, scale = :log)
    sigma_C  = RealNumber(1.0, scale = :log)
    sigma_kout = RealNumber(0.3, scale = :log)
    sigma_R   = RealNumber(5.0, scale = :log)
    ml_params = NNParameters(chainE; function_name = :ML)
end
@covariates begin
    t = Covariate()
    d = ConstantCovariate(; constant_on = :id)
    wt = ConstantCovariate(; constant_on = :id)
    R0 = ConstantCovariate(; constant_on = :id)
end
@randomEffects begin
    ka = RandomEffect(LogNormal(ka_mean, sigma_ka); column = :id)
    CL = RandomEffect(
        LogNormal(CL_mean + 0.75 * log(wt / 70.0), sigma_CL);
        column = :id)
    V = RandomEffect(LogNormal(V_mean, sigma_V); column = :id)
    kout = RandomEffect(LogNormal(kout_mean, sigma_kout); column = :id)
end
@DifferentialEquation begin
    eff(t) = (center / V) *
        softplus(ML([(center / V) / 5.0], ml_params)[1])
    D(depot) ~ -ka * depot
    D(center) ~ ka * depot - (CL / V) * center
    D(response) ~ kout * (R0 - response * (1 + eff(t)))
end
@initialDE begin
    depot = d; center = 0.0; response = R0
end
@formulas begin
    C ~ Normal(center(t) / V, sigma_C)
    R ~ Normal(response(t), sigma_R)
end
end
end

```

The soft-tree model has the same structure and differs only in the effect component. Because the `@Model` macro can extend an existing model, the soft-tree model is obtained from the

neural model by overriding a single fixed effect:

```
model_st = @Model model_nn begin
  @fixedEffects begin
    ml_params = SoftTreeParameters(1, 2; function_name = :ML)
  end
end
```

Reusing the function name `:ML` leaves the differential-equation, observation, and random-effect blocks of `model_nn` unchanged, so swapping the network for a depth-two soft decision tree is a few-line change that leaves all other model components unchanged.

6.2.2 Cross-validated comparison

In the following example, we compare the three models using 10-fold leave-subjects-out CV. In each fold, entire subjects are held out and their responses are predicted from the population distribution, mimicking prediction for a new patient. Performance is evaluated by the mean squared error of the held-out INR response via the `loss` argument. We score INR rather than concentration because the PK submodel is identical across all models, so only the PD component differs. Setting `store_results = true` retains the fitted models from each fold, allowing the learned effect function, predicted response, and their cross-validation uncertainty to be reconstructed. The soft-tree model `model_st` and the parametric `Emax` reference of Appendix B.2 are bound to the same data and cross-validated with identical calls, so the three results are directly comparable:

```
dm_nn = DataModel(model_nn, df; primary_id = :id, time_col = :t)
mse_loss = (dist, y) -> (mean(dist) - y)^2

cv = cross_validate(dm_nn, 10; kind = :id, rng = MersenneTwister(1))
fit = fit_cv(cv, SAEM(maxiters = 200);
  unseen_re_mode = :mean, loss = mse_loss, store_results = true,
  rng = MersenneTwister(2))
```

The INR response declines after dosing and recovers as warfarin clears, with greater between-subject variability during recovery (Figure 5A). The estimated concentration-effect relationships carry the main finding of the analysis (Figure 5C). The neural network and soft tree, fitted independently, recover similar threshold-shaped effects that remain close to zero below roughly 4 mg/L before increasing steeply, a qualitatively different shape from the gradual response implied by the parametric `Emax` model. This learned shape is the diagnostic payoff

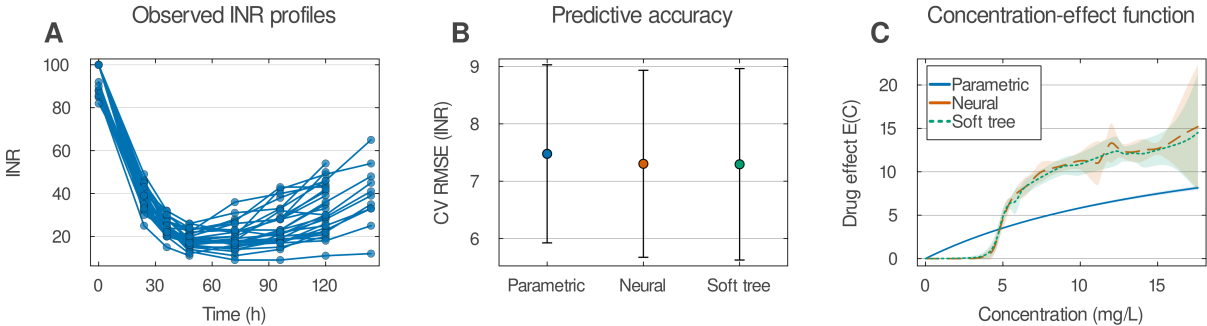


Figure 5: Warfarin anticoagulant response and pharmacodynamic model comparison. (A) Observed INR responses over time for all subjects. (B) Cross-validated RMSE on the held-out INR response for each model under 10-fold leave-subjects-out cross-validation (mean and 95% confidence interval across folds). (C) Estimated concentration-effect function $\mathcal{E}(C)$ for the parametric E_{\max} model and the learned neural-network and soft-tree effects, with pointwise 95% confidence bands across folds.

of the flexible components, because the agreement of two independent function approximators on a threshold form is stronger evidence for that form than either model alone, and it identifies a plausible alternative to the saturable E_{\max} assumption that a purely parametric workflow would not surface. The three models nonetheless achieve nearly identical held-out performance, with overlapping cross-validated RMSE intervals (Figure 5B), because the effect shape trades off against the turnover rate k_{out} . The E_{\max} model compensates for its gradual effect with a turnover rate of 0.0086 h^{-1} [0.0084, 0.0088], approximately twice that of the neural network (0.0040 [0.0036, 0.0043]) and soft tree (0.0041 [0.0037, 0.0046]), so all three generate nearly identical INR predictions despite markedly different concentration-effect curves. The flexible models therefore do not improve prediction on this dataset, but they earn their place as a diagnostic that reveals structure in the concentration-effect relationship, a conclusion that remains suggestive rather than definitive because the flexible models do not share the E_{\max} parameterization.

6.3 Fish growth: normalizing flows as flexible random-effects distributions

The previous two examples relied on Gaussian random effects. Partial migration can instead produce multimodal growth-rate distributions that violate this assumption [Hegemann et al., 2019]. Normalizing flows address this by learning flexible, potentially multimodal random-effects distributions from the data. In **NoLimits.jl**, a normalizing flow can directly replace a Gaussian random-effects distribution without changing the rest of the model. We compare Gaussian and flow-based random-effects models on simulated data using SAEM.

6.3.1 Data

The dataset of Gillanders et al. [2015] comprises individual growth records for 167 black bream (*Acanthopagrus butcheri*), a long-lived estuarine sparid, sampled in the Coorong Estuary, South Australia, between 2008 and 2012. Captured fish span ages 5 to 32 years and lengths of 283 to 470 mm, and the original study classified each fish as resident (104) or migratory (63) from otolith microchemistry, a partial-migration structure that motivates a multimodal growth-rate distribution. Rather than fitting these records directly, we use them to calibrate a realistic simulation in which the true random-effects distribution is known, so that the recovery of latent sub-population structure can be assessed against a ground truth (Section 6.3.3). The simulated morph labels are withheld from every estimation model and retained only to color the figures, so any recovered bimodality must emerge from the fitted growth trajectories alone.

6.3.2 Model specification

We model length at age with a von Bertalanffy growth function (VBGF) [von Bertalanffy, 1957]. For fish $i = 1, \dots, N$ observed at ages t_{ij} , $j = 1, \dots, n_i$, length L_{ij} is described by

$$L_{ij} \mid L_{\infty,i}, k_i \sim \mathcal{N}\left(L_{\infty,i}\left(1 - e^{-k_i t_{ij}}\right), \sigma_y^2\right), \quad (22)$$

$$L_{\infty,i} = L_{\infty,\text{pop}} e^{b_{L,i}}, \quad b_{L,i} \sim \mathcal{N}(0, \sigma_L^2), \quad (23)$$

$$k_i = k_{\text{pop}} e^{b_{k,i}}, \quad b_{k,i} \sim \mathcal{D}, \quad (24)$$

where $L_{\infty,\text{pop}} > 0$ is the population-level asymptotic length, $k_{\text{pop}} > 0$ is the population-level growth-rate coefficient, $\sigma_L > 0$ controls inter-individual variability in asymptotic length, and $\sigma_y > 0$ is the residual standard deviation. The asymptotic-length random effect $b_{L,i}$ is Gaussian throughout, whereas the growth-rate random effect $b_{k,i}$ is drawn from a distribution \mathcal{D} that we deliberately leave unspecified at this stage. This distribution is the single component that varies across the remainder of the section. We first instantiate \mathcal{D} as a known bimodal mixture to generate simulated data (Section 6.3.3), then estimate it from those data under two competing assumptions, a Gaussian family and a flexible normalizing flow (Section 6.3.4).

6.3.3 Data simulation

To test whether a flexible random-effects distribution recovers latent structure when it is genuinely present, we simulate from the model of Equations 22–24 with \mathcal{D} set to a known bimodal distribution

$$b_{k,i} \sim \frac{1}{2} \mathcal{N}(-\mu, \sigma_c^2) + \frac{1}{2} \mathcal{N}(\mu, \sigma_c^2), \quad \mu = 0.70, \quad \sigma_c = 0.20, \quad (25)$$

representing a slow-growing morph centered at $-\mu$ and a fast-growing morph centered at μ . The data-generating parameters are calibrated to the real Gillanders et al. [2015] data by a Gaussian SAEM fit, giving an asymptotic length near 705 mm, growth coefficient near 0.104 year^{-1} , and residual standard deviation near 15 mm.

In **NoLimits.jl** the mixture is realized through a binary covariate `morph` that selects the component mean, so that over an even split of morphs the marginal distribution of $b_{k,i}$ matches Equation 25. The `morph` label is supplied only to the simulation model and withheld from every estimation model, which observes only `fishid`, `age`, and `length`, so any recovered bimodality must emerge from the fitted growth curves rather than from a known grouping. The simulation model encodes the mixture in its `@randomEffects` block:

```

model_sim = @Model begin
  @covariates begin
    age = Covariate()
    morph = ConstantCovariate(; constant_on = :fishid)
  end
  @fixedEffects begin
    L_inf_pop = RealNumber(705.0, scale = :log)
    k_pop = RealNumber(0.104, scale = :log)
    sigma_L = RealNumber(0.10, scale = :log)
    sigma_y = RealNumber(15.0, scale = :log)
    mu_bim = RealNumber(0.70)
    sigma_comp = RealNumber(0.20, scale = :log)
  end
  @randomEffects begin
    b_k = RandomEffect(Normal((2 * morph - 1) * mu_bim, sigma_comp);
      column = :fishid)
    b_L = RandomEffect(Normal(0.0, sigma_L); column = :fishid)
  end
  @formulas begin
    length ~ Normal(
      L_inf_pop * exp(b_L) *
      (1 - exp(- k_pop * exp(b_k) * age)),
      sigma_y)
  end
end
end

```

The component-mean term $(2 * \text{morph} - 1) * \text{mu_bim}$ evaluates to $-\mu$ for `morph = 0` and μ for `morph = 1`, encoding the mixture of Equation 25. The model is attached to a template

DataFrame of 100 fish split evenly between the morphs and observed at ages 2–15 years, constructed as shown in the replication materials. Observations are drawn with `simulate_data`, the **NoLimits.jl** function that samples the random effects from the prior and appends their true values to the returned DataFrame:

```
dm_sim = DataModel(model_sim, df_template;
                   primary_id = :fishid, time_col = :age)
df_sim = simulate_data(dm_sim; rng = MersenneTwister(42))
```

The simulated length-at-age trajectories separate into two bundles, the fast morph reaching markedly larger lengths than the slow morph, yet they overlap at the youngest ages where growth has not yet diverged, so the morph of an individual fish is not perfectly identifiable from its trajectory alone. The marginal density of the growth-rate random effect is the equally weighted bimodal mixture of Equation 25, the latent structure that a Gaussian random-effects distribution cannot represent and that the normalizing flow is designed to recover. It appears as the dashed reference in Figure 6A.

6.3.4 Model fitting and comparison

We now instantiate \mathcal{D} in two estimation models and fit both to the simulated data with SAEM. The Gaussian baseline places

$$b_{k,i} \sim \mathcal{N}(0, \sigma_k^2), \quad (26)$$

with $\sigma_k > 0$, while the flow model replaces Equation 26 with a normalizing planar flow p_ψ parameterized by weights ψ , whose density follows the change-of-variables form of Equation 3. The complete parameter vector is $\theta = (L_{\infty, \text{pop}}, k_{\text{pop}}, \sigma_L, \sigma_y, \sigma_k)$ for the Gaussian model and $\theta = (L_{\infty, \text{pop}}, k_{\text{pop}}, \sigma_L, \sigma_y, \psi)$ for the flow model. The Gaussian specification translates directly into the `@Model` macro:

```
model_gauss = @Model begin
  @covariates begin; age = Covariate(); end
  @fixedEffects begin
    L_inf_pop = RealNumber(705.0, scale = :log)
    k_pop     = RealNumber(0.104, scale = :log)
    sigma_L   = RealNumber(0.10,  scale = :log)
    sigma_k   = RealNumber(0.40,  scale = :log)
    sigma_y   = RealNumber(15.0,  scale = :log)
  end
end
```

```

@randomEffects begin
  b_k = RandomEffect(Normal(0.0, sigma_k); column = :fishid)
  b_L = RandomEffect(Normal(0.0, sigma_L); column = :fishid)
end
@formulas begin
  length ~ Normal(
    exp(log(L_inf_pop) + b_L) *
    (1 - exp(-exp(log(k_pop) + b_k) * age)),
    sigma_y)
end
end
end

```

The normalizing flow specification makes three targeted changes to the Gaussian model: `sigma_k` is replaced by `NPFParameter(1, 4; seed = 42, calculate_se = false)`, which parameterizes the weights of four successive planar transformation layers, the `b_k` random effect distribution is specified as `NormalizingPlanarFlow(psi)` in place of a Gaussian distribution, and the random effect is now a vector, so it is indexed with square brackets as `b_k[1]` in the formula. All remaining declarations match `model_gauss`, so these three changes define `model_flow`. Both specifications are attached to the simulated data via `DataModel`:

```

dm_gauss = DataModel(model_gauss, df_sim;
  primary_id = :fishid, time_col = :age)
dm_flow = DataModel(model_flow, df_sim;
  primary_id = :fishid, time_col = :age)

```

Both models are fit with SAEM for 800 iterations. The flow's `k_pop` is held at the Gaussian estimate through the `constants` keyword, because the flow random effect, unlike the Gaussian one, is not constrained to be centered at zero. A location shift can therefore move freely between `k_pop` and the random-effect distribution, leaving the two not jointly identifiable. The fitted fixed effects are then placed side by side with `compare_parameters`, which aligns the parameters shared by the two models and marks with a dash any parameter that one model does not have:

```

Random.seed!(42)
fit_gauss = fit_model(dm_gauss, SAEM(maxiters = 800))
fit_flow = fit_model(dm_flow, SAEM(maxiters = 800);
  constants = (k_pop = get_params(fit_gauss).k_pop,))
compare_parameters(fit_gauss, fit_flow; labels = ["Gaussian", "flow"])

```

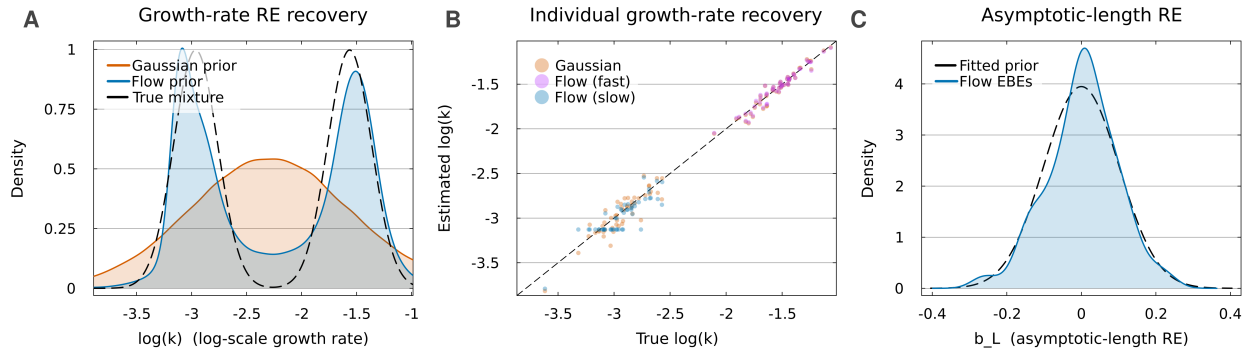


Figure 6: Random-effect distribution recovery on simulated data. (A) Fitted growth-rate random-effect priors on the $\log(k)$ scale: the true generating mixture (black dashed), the fitted Gaussian prior (red), and the fitted normalizing-flow prior (blue filled). Both fitted priors are shown as kernel density estimates of draws from the corresponding random-effect distribution. (B) Estimated versus true $\log(k)$ for both models, with flow-model EBEs colored by true morph (orange: fast, blue: slow), Gaussian-model EBEs in red, and the identity line dashed. (C) Flow-model EBEs for the asymptotic-length random effect b_L (blue) overlaid on the fitted Gaussian prior (black dashed).

ParameterComparison

parameter	Gaussian	flow
L_inf_pop	718.4175	703.1301
k_pop	0.1014	0.1014
sigma_L	0.1083	0.1208
sigma_k	0.7272	-
sigma_y	15.4	15.3597

The two models recover markedly different random-effect priors (Figure 6A). The Gaussian prior is unimodal and places substantial density between the two true modes, whereas the flow recovers the underlying bimodal structure. Both models estimate individual growth-rate EBEs with similar accuracy (Figure 6B), indicating that the data are sufficiently informative at the individual level. The main advantage of the flow therefore lies in its population-level representation: samples from the flow reproduce both subpopulations, while samples from the Gaussian prior concentrate unrealistically between them. In contrast, the asymptotic-length random effect b_L , modeled as Gaussian in both cases, is recovered consistently (Figure 6C), demonstrating that Gaussian and flow-based random effects can be combined within the same model.

`plot_random_effects_pdf(fit_gauss; re_names = :b_k, style = my_style)`

```
plot_random_effects_pdf(fit_flow; re_names = :b_k, style = my_style)
```

7 Comparison to other software packages

This section positions **NoLimits.jl** within the open-source ecosystem for NLME and longitudinal modeling.

7.1 Scope and the open-source landscape

We restrict the comparison to open-source software. Commercial tools such as **NONMEM** [Bauer, 2019], **Monolix** [Simulations Plus, 2024], and **Pumas** [Rackauckas et al., 2020b] are therefore excluded. Among these, **Pumas** offers a comparably broad range of model classes, random-effects distributions, and inference paradigms. Thus, the contribution of **NoLimits.jl** is best understood as making a similar breadth of capabilities available in an open-source framework, rather than as introducing all of these capabilities for the first time. We also do not compare directly against general-purpose probabilistic programming languages such as **Stan** [Stan Development Team, 2026], **Turing.jl** [Ge et al., 2018, Fjelde et al., 2025], and **PyMC** [Abril-Pla et al., 2023]. These provide flexible inference engines rather than domain-specific NLME frameworks. In particular, **NoLimits.jl** builds on **Turing.jl** for Bayesian inference, generating **Turing.jl** models at runtime and reusing its sampling algorithms. Rather than competing with these tools, **NoLimits.jl** provides a higher-level modeling framework that integrates mixed-effects, ODE, and Markov models together with specialized estimation and diagnostic methods.

The most closely related open-source packages are the R packages **nlmixr2** [Fidler, 2025] and **saemix** [Comets et al., 2017], which focus on pharmacometric mixed-effects modeling, as well as specialized latent-state packages such as **mHMMbayes** [Aarts and Mildiner Moraga, 2026]. The remainder of this section compares **NoLimits.jl** primarily with **nlmixr2** and **saemix**. As summarized in Table 5, **NoLimits.jl** unifies a broader range of model classes, random-effects distributions, learned components, and inference paradigms within a single composable framework.

7.2 Close comparison: **nlmixr2** and **saemix**

nlmixr2 [Fidler, 2025] and **saemix** [Comets et al., 2017] are mature and widely used pharmacometric R packages centered on SAEM and, for **nlmixr2**, also FOCEI. The differences discussed below are therefore primarily differences in scope: **nlmixr2** and **saemix** focus on pharmacometric workflows, whereas **NoLimits.jl** emphasizes breadth across model classes,

Feature	NoLimits.jl	nlmixr2	saemix	Feature	NoLimits.jl	nlmixr2	saemix
<i>Model classes</i>				<i>Machine Learning</i>			
ODE-based models	✓	✓	(✓) ^a	Neural Networks	✓	(✓) ^e	–
Closed-form models	✓	✓	✓	Soft Trees	✓	–	–
Markov models	✓	–	–	<i>Inference and uncertainty</i>			
Time-to-event, censored	✓	✓	✓	Likelihood / EM	✓	✓	✓
<i>Random effects</i>				Bayesian (MCMC)	✓	–	–
Gaussian	✓	✓	✓	Bootstrap uncertainty	–	✓	✓
Skewed	✓	✓ ^b	✓ ^c	Automated covariate search	–	✓	–
Heavy-tailed (t , Laplace)	✓	–	–	<i>Platform and ecosystem</i>			
Normalizing-flow	✓	–	–	Language	Julia	R	R
<i>Observation models</i>				Open-source	✓	✓	✓
Non-Gaussian observations	✓	✓	✓ ^d	NONMEM/Monolix import	–	✓	–

Table 5: Feature comparison of **NoLimits.jl**, **nlmixr2**, and **saemix**. Check marks denote native support, bracketed check marks conditional or extension-based support, and dashes no readily available support in the standard workflow. ^a External ODE solver. ^b Transformation-based support. ^c Via `transform.par`. ^d Via user-defined likelihoods [Comets et al., 2026]. ^e Via **pmxNODE** [Bräm, 2025]. Versions: **NoLimits.jl** 0.1.0, **nlmixr2** 4.0.1, **saemix** 3.5.

random-effects distributions, learned components, and inference paradigms for general and neural NLME.

Table 5 summarizes the main differences. The most pronounced distinction lies in the random-effects distribution. **nlmixr2** and **saemix** support Gaussian and transformed distributions such as the log-normal, but not symmetric heavy-tailed or flow-based random effects. **NoLimits.jl** additionally supports Student’s t , Laplace, and normalizing-flow distributions, enabling flexible and multimodal random-effects models as illustrated in Section 6.3.

The supported model classes also differ. Neither **nlmixr2** nor **saemix** provides native support for Markov models, whereas **NoLimits.jl** includes discrete- and continuous-time Markov observation models with hidden or observed states within the same framework.

Neural-network integration is another point of departure. Through the third-party **pmxN-ODE** package [Bräm, 2025], **nlmixr2** supports a restricted class of neural-ODE models, while **saemix** offers no direct neural-network support. In contrast, **NoLimits.jl** integrates arbitrary **Lux.jl** and **SimpleChains.jl** networks, as well as differentiable soft trees as composable model components that can appear in structural, observation, and random-effects models.

Finally, **NoLimits.jl** unifies likelihood-based, EM-based, and Bayesian inference behind a common interface, including MCMC through its **Turing.jl** backend. Neither **nlmixr2** nor **saemix** provides Bayesian MCMC inference.

These advantages in flexibility are balanced by strengths of the incumbents. **nlmixr2** and **saemix** benefit from extensive validation, large user communities, and pharmacometric workflow tooling such as bootstrap uncertainty quantification, automated covariate search, and interoperability with established tools. For workflows that depend on this ecosystem, they remain compelling choices.

7.3 Decision guidance

In summary, the comparison above points to complementary strengths. **nlmixr2** and **saemix** [Fidler, 2025, Comets et al., 2017] remain natural choices for established pharmacometric workflows that rely on their mature ecosystems and extensive validation, whereas **NoLimits.jl** targets the broader modeling and inference space of Table 5, in particular Markov models, flexible random-effects distributions, native neural-network components, and exploratory development under a unified likelihood-and-Bayesian interface. For fully bespoke Bayesian models outside the mixed-effects setting, users can access the underlying **Turing.jl** backend directly [Ge et al., 2018, Fjelde et al., 2025].

8 Conclusions

We introduced **NoLimits.jl**, an open-source Julia framework that places classical mixed-effects models, mechanistic systems, and hybrid mechanistic–neural formulations under a single composable modeling and inference interface. A macro-based language specifies observation models as parameterized conditional distributions whose random effects are drawn from the **Distributions.jl** ecosystem and may be Gaussian, heavy-tailed, or flow-based with covariate-dependent parameters, while neural networks, differentiable soft trees, and differentiable ODE solvers act as first-class building blocks for any part of a model. Laplace approximation, the stochastic EM algorithms SAEM and MCEM, maximum likelihood, and full Bayesian inference through **Turing.jl** are all reachable from the same specification, together with simulation, uncertainty quantification, predictive checks, diagnostics, and cross-validation. We demonstrated this breadth on a warfarin population pharmacokinetic model, a learnable concentration-effect function for the pharmacodynamics of the same drug, and normalizing-flow random effects in a fish-growth study. Across the three studies, the flexible components proved valuable less for improving individual-level prediction than for revealing structure that rigid parametric assumptions obscure, namely the learned concentration-effect shape in the pharmacodynamic example and the recovered bimodal random-effects distribution in the growth model.

To the best of our knowledge, **NoLimits.jl** is the only open-source NLME framework that combines ODE and Markov model classes, heavy-tailed and flow-based random effects, native neural-network components with automatic differentiation, and a unified likelihood-and-Bayesian inference interface, broadening the modeling and inference design space relative to the established packages **nlmixr2** and **saemix**. This breadth comes at the cost of maturity. **NoLimits.jl** does not yet match their extensive validation record or large pharmacometrics ecosystems, and it currently lacks some of their workflow tooling, including bootstrap-based parameter uncertainty, automated stepwise covariate selection, and import and export of **NONMEM** and **Monolix** models.

Closing these gaps, broadening the catalog of built-in model components, and growing the body of validation studies are the focus of ongoing development. The default forward-mode automatic differentiation, required by the nested optimization within the Laplace and FOCEI estimators, remains efficient up to roughly one hundred parameters and so covers many practical applications, while substantially larger models would benefit from reverse-mode differentiation, for which planned variational inference over the random effects [Arruda et al., 2024, Tarek and Afonso, 2026] is a promising route. Further plans include privacy-preserving analysis such as federated learning [McMahan et al., 2017] via DataSHIELD [Wilson et al., 2017]. **NoLimits.jl** is released under the MIT license and developed openly at <https://github.com/manuhuth/NoLimits.jl>. We invite the community to apply the framework to

new problems, report issues, and contribute model components, inference procedures, and examples.

Acknowledgments

This study received financial support by the German Research Foundation (Deutsche Forschungsgemeinschaft, DFG) under Germany’s Excellence Strategy (EXC 2047 - 390685813 and EXC 2151 - 390873048), the University of Bonn (via the Schlegel Professorship of JH), and by the European Union. Views and opinions expressed are however those of the author(s) only and do not necessarily reflect those of the European Union or the European Research Council Executive Agency. Neither the European Union nor the granting authority can be held responsible for them. This work is supported by ERC grant INTEGRATE, grant agreement number 101126146.

The funders had no role in the study design, data collection, data analyses, data interpretation, writing, or submission of this manuscript.

Author contributions

M.H. conceptualized the framework, designed and implemented the **NoLimits.jl** software package, and wrote the manuscript. V.W. implemented the directed-acyclic-graph-based improvements for the Markov models. R.G. assisted with the theory for the hidden Markov model implementation and tested the hidden Markov model examples. N.S. conducted universal differential equation experiments and created Figure 1. C.P. contributed real-world ordinary differential equation benchmarks during development. J.A. provided methodological input on normalizing flows, tested and benchmarked the corresponding capabilities. J.H. acquired funding and supervised the work. All authors read and approved the final manuscript.

Code availability and reproducibility

NoLimits.jl is open-source software released under the MIT license and developed publicly at <https://github.com/manuhuth/NoLimits.jl>. The results reported in this article were produced with **NoLimits.jl** version 0.1.0 under Julia 1.12.1.

All material required to reproduce the results is archived on Zenodo at <https://doi.org/10.5281/zenodo.20797370>. The archive contains the replication script `replication.jl` together with the `Project.toml` and `Manifest.toml` files that pin the exact versions of all

dependencies. Executing the script in the provided environment regenerates every figure reported in this article.

Declaration of generative AI

NoLimits.jl was developed with substantial assistance from large language models, primarily Anthropic’s Claude (via Claude Code), for code generation, refactoring, test authoring, and documentation. All contributions were reviewed, tested, and are understood by the maintainers, who take full responsibility for the package. This is disclosed per the Julia General Registry’s guidance on AI-assisted packages.

During the preparation of this manuscript, the authors used Claude and ChatGPT to correct grammar and spelling and to improve the style of writing. After using these tools, the authors reviewed and edited the content as needed and take full responsibility for the content of this manuscript.

References

- E. Aarts and S. Mildiner Moraga. *mHMMbayes: Multilevel Hidden Markov Models Using Bayesian Estimation*, 2026. URL <https://github.com/emmekeaarts/mhmmbayes>. R package version 1.1.1.
- O. Abril-Pla, V. Andreani, C. Carroll, L. Dong, C. J. Fonnesebeck, M. Kochurov, R. Kumar, J. Lao, C. C. Luhmann, O. A. Martin, M. Osthege, R. Vieira, T. Wiecki, and R. Zinkov. PyMC: A modern and comprehensive probabilistic programming framework in Python. *PeerJ Computer Science*, 9(e1516), 2023. doi: 10.7717/peerj-cs.1516.
- J. Arruda, Y. Schälte, C. Peiter, O. Tepytska, U. Jaehde, and J. Hasenauer. An amortized approach to non-linear mixed-effects modeling based on neural posterior estimation. In *Proceedings of the 41st International Conference on Machine Learning*, pages 1865–1901, 2024.
- D. Bates, M. Mächler, B. Bolker, and S. Walker. Fitting linear mixed-effects models using lme4. *Journal of Statistical Software*, 67(1):1–48, 2015. doi: 10.18637/jss.v067.i01.
- R. J. Bauer. Nonmem tutorial part i: description of commands and options, with simple examples of population analysis. *CPT: Pharmacometrics & Systems Pharmacology*, 8(8): 525–537, 2019. doi: 10.1002/psp4.12404.

- M. Bergstrand, A. C. Hooker, J. E. Wallin, and M. O. Karlsson. Prediction-corrected visual predictive checks for diagnosing nonlinear mixed-effects models. *The AAPS Journal*, 13(2):143–151, 2011. doi: 10.1208/s12248-011-9255-z.
- M. Besançon, T. Papamarkou, D. Anthoff, A. Arslan, S. Byrne, D. Lin, and J. Pearson. Distributions.jl: Definition and modeling of probability distributions in the JuliaStats ecosystem. *Journal of Statistical Software*, 98(16):1–30, 2021. doi: 10.18637/jss.v098.i16.
- J. Bezanson, A. Edelman, S. Karpinski, and V. B. Shah. Julia: A fresh approach to numerical computing. *SIAM review*, 59(1):65–98, 2017. doi: 10.1137/141000671.
- S. Bhagavan, B. de Koning, S. Maddhashiya, and C. Rackauckas. Datainterpolations.jl: Fast interpolations of 1d data. *Journal of Open Source Software*, 9(101):6917, 2024. doi: 10.21105/joss.06917.
- D. M. Blei, A. Kucukelbir, and J. D. McAuliffe. Variational inference: A review for statisticians. *Journal of the American statistical Association*, 112(518):859–877, 2017. doi: 10.1080/01621459.2017.1285773.
- I. Borisov, A. Demin, and E. Metelkin. LikelihoodProfiler.jl: Unified profile-likelihood workflows for identifiability and confidence intervals. *Journal of Open Source Software*, 11(117):9501, 2026. doi: 10.21105/joss.09501.
- M. Bouchet-Valat and B. Kamiński. Dataframes.jl: Flexible and fast tabular data in julia. *Journal of Statistical Software*, 107(4):1–32, 2023. doi: 10.18637/jss.v107.i04.
- D. Bräm. *pmxNODE: Application of NODEs in Monolix, NONMEM, and nlmixr2*, 2025. URL <https://CRAN.R-project.org/package=pmxNODE>. R package version 0.1.0.
- D. S. Bräm, B. Steiert, M. Pfister, B. Steffens, and G. Koch. Low-dimensional neural ordinary differential equations accounting for inter-individual variability implemented in Monolix and NONMEM. *CPT: Pharmacometrics & Systems Pharmacology*, 14(1):5–16, 2025. doi: 10.1002/psp4.13265.
- T. Breloff et al. Plots.jl, 2026. Julia package version 1.41.6.
- S. Chib and E. Greenberg. Understanding the metropolis-hastings algorithm. *The American Statistician*, 49(4):327–335, 1995. doi: 10.1080/00031305.1995.10476177.
- S. Chung and L. Cai. Cross-classified random effects modeling for moderated item calibration. *Journal of Educational and Behavioral Statistics*, 46(6):651–681, 2021. doi: 10.3102/1076998620983908.

- P. M. Cogswell, E. S. Lundt, T. M. Therneau, C. T. Mester, H. J. Wiste, J. Graff-Radford, C. G. Schwarz, M. L. Senjem, J. L. Gunter, R. I. Reid, et al. Evidence against a temporal association between cerebrovascular disease and alzheimer’s disease imaging biomarkers. *Nature communications*, 14(1):3097, 2023. doi: 10.1038/s41467-023-38878-8.
- E. Comets, A. Lavenu, and M. Lavielle. Parameter estimation in nonlinear mixed effect models using saemix, an r implementation of the saem algorithm. *Journal of Statistical Software*, 80:1–41, 2017. doi: 10.18637/jss.v080.i03.
- E. Comets, M. Delattre, and B. Karimi. Extending the saemix package for R to fit non gaussian outcomes. *arXiv preprint arXiv:2603.03154*, 2026.
- M. Davidian and D. M. Giltinan. Nonlinear models for repeated measurement data: an overview and update. *Journal of agricultural, biological, and environmental statistics*, 8(4):387–419, 2003. doi: 10.1198/1085711032697.
- N. L. Dayneka, V. Garg, and W. J. Jusko. Comparison of four basic models of indirect pharmacodynamic responses. *Journal of pharmacokinetics and biopharmaceutics*, 21(4):457–478, 1993. doi: 10.1007/BF01061691.
- B. Delyon, M. Lavielle, and E. Moulines. Convergence of a stochastic approximation version of the em algorithm. *Annals of statistics*, pages 94–128, 1999. doi: 10.1214/aos/1018031103.
- A. P. Dempster, N. M. Laird, and D. B. Rubin. Maximum likelihood from incomplete data via the em algorithm. *Journal of the royal statistical society: series B (methodological)*, 39(1):1–22, 1977. doi: 10.1111/j.2517-6161.1977.tb01600.x.
- V. K. Dixit and C. Rackauckas. *Optimization.jl: A Unified Optimization Package*, 2023. URL <https://doi.org/10.5281/zenodo.7738525>.
- A. El-Gazzar and M. van Gerven. Universal differential equations as a unifying modeling language for neuroscience. *Frontiers in Computational Neuroscience*, 19:1677930, 2025. doi: 10.3389/fncom.2025.1677930.
- R. Feldt and A. Stukalov. *BlackBoxOptim.jl: Black-Box Optimization in Julia*, 2026. URL <https://github.com/robertfeldt/BlackBoxOptim.jl>. Julia package version 0.6.5.
- M. Fidler. *nlmixr2: Nonlinear Mixed Effects Models in Population PK/PD*, 2025. URL <https://CRAN.R-project.org/package=nlmixr2>. R package version 4.0.1.
- R. A. Fisher. Theory of statistical estimation. *Mathematical Proceedings of the Cambridge Philosophical Society*, 22(5):700–725, 1925. doi: 10.1017/S0305004100009580.

- T. E. Fjelde, K. Xu, D. Widmann, M. Tarek, C. Pfiffer, M. Trapp, S. D. Axen, X. Sun, M. Hauru, P. Yong, W. Tebbutt, Z. Ghahramani, and H. Ge. Turing.jl: a general-purpose probabilistic programming language. *ACM Trans. Probab. Mach. Learn.*, Feb. 2025. doi: 10.1145/3711897. URL <https://doi.org/10.1145/3711897>. Just Accepted.
- F. Fröhlich, B. Kaltenbacher, F. J. Theis, and J. Hasenauer. Scalable parameter estimation for genome-scale biochemical reaction networks. *PLoS computational biology*, 13(1):e1005331, 2017. doi: 10.1371/journal.pcbi.1005331.
- H. Ge, K. Xu, and Z. Ghahramani. Turing: A language for flexible probabilistic inference. In A. Storkey and F. Perez-Cruz, editors, *Proceedings of the Twenty-First International Conference on Artificial Intelligence and Statistics*, volume 84 of *Proceedings of Machine Learning Research*, pages 1682–1690. PMLR, 09–11 Apr 2018. URL <https://proceedings.mlr.press/v84/ge18b.html>.
- A. E. Gelfand and A. F. Smith. Sampling-based approaches to calculating marginal densities. *Journal of the American statistical association*, 85(410):398–409, 1990. doi: 10.1080/01621459.1990.10476213.
- A. Gelman, J. B. Carlin, H. S. Stern, and D. B. Rubin. *Bayesian data analysis*. Chapman and Hall/CRC, 1995.
- A. Gelman, J. B. Carlin, H. S. Stern, D. B. Dunson, A. Vehtari, and D. B. Rubin. *Bayesian Data Analysis (3rd Edition)*. Chapman and Hall/CRC, 2013. doi: 10.1201/b16018. URL <https://doi.org/10.1201/b16018>.
- B. M. Gillanders, C. Izzo, Z. A. Doubleday, and Q. Ye. Partial migration: Growth varies between resident and migratory fish. *Biology Letters*, 11(3):20140850, 2015. doi: 10.1098/rsbl.2014.0850.
- J. V. Gobburu. Pharmacometrics 2020. *The Journal of Clinical Pharmacology*, 50(S9): 151S–157S, 2010. doi: 10.1177/0091270010376977.
- I. Goodfellow, Y. Bengio, and A. Courville. *Deep Learning*. MIT Press, Cambridge, 2016.
- M. D. Greenberg. *Foundations of Applied Mathematics*. Courier Corporation, 2013.
- P. Hartman. *Ordinary Differential Equations*. Society for Industrial and Applied Mathematics, 2002. doi: 10.1137/1.9780898719222.
- A. Hegemann, A. M. Fudickar, and J.-Å. Nilsson. A physiological perspective on the ecology and evolution of partial migration. *Journal of Ornithology*, 160(3):893–905, 2019. doi: 10.1007/s10336-019-01648-9.

- M. D. Hoffman, A. Gelman, et al. The no-u-turn sampler: adaptively setting path lengths in hamiltonian monte carlo. *J. Mach. Learn. Res.*, 15(1):1593–1623, 2014.
- A. C. Hooker, C. E. Staats, and M. O. Karlsson. Conditional weighted residuals (CWRES): A model diagnostic for the FOCE method. *Pharmaceutical Research*, 24(12):2187–2197, 2007. doi: 10.1007/s11095-007-9361-x.
- K. Hornik, M. Stinchcombe, and H. White. Multilayer feedforward networks are universal approximators. *Neural Networks*, 2(5):359–366, 1989. doi: 10.1016/0893-6080(89)90020-8.
- M. Innes. Flux: Elegant machine learning with julia. *Journal of Open Source Software*, 2018. doi: 10.21105/joss.00602.
- O. Irsoy, O. T. Yıldız, and E. Alpaydın. Soft decision trees. In *Proceedings of the 21st International Conference on Pattern Recognition (ICPR2012)*, pages 1819–1822. IEEE, 2012.
- S. G. Johnson. The NLOpt nonlinear-optimization package. <https://github.com/stevengj/nlopt>, 2007.
- M. O. Karlsson, S. L. Beal, and L. B. Sheiner. Three new residual error models for population pk/pd analyses. *Journal of pharmacokinetics and biopharmaceutics*, 23(6):651–672, 1995. doi: 10.1007/BF02353466.
- E. Kuhn and M. Lavielle. Coupling a stochastic approximation version of em with an mcmc procedure. *ESAIM: Probability and Statistics*, 8:115–131, 2004. doi: 10.1051/ps:2004007.
- E. Kuhn and M. Lavielle. Maximum likelihood estimation in nonlinear mixed effects models. *Computational Statistics & Data Analysis*, 49(4):1020–1038, 2005. doi: 10.1016/j.csda.2004.07.002.
- S. Lane, S. Al-Zubiedi, E. Hatch, I. Matthews, A. L. Jorgensen, P. Deloukas, A. K. Daly, B. K. Park, L. Aarons, K. Ogungbenro, et al. The population pharmacokinetics of R- and S-warfarin: Effect of genetic and clinical factors. *British Journal of Clinical Pharmacology*, 73(1):66–76, 2012. doi: 10.1111/j.1365-2125.2011.04051.x.
- M. Lavielle. *Mixed effects models for the population approach: models, tasks, methods and tools*. CRC press, 2014. doi: 10.1201/b17203.
- M. J. Lindstrom and D. M. Bates. Nonlinear mixed effects models for repeated measures data. *Biometrics*, pages 673–687, 1990. doi: 10.2307/2532087.
- D. C. Liu and J. Nocedal. On the limited memory BFGS method for large scale optimization. *Mathematical Programming*, 45(1):503–528, 1989. doi: 10.1007/BF01589116.

- D. J. Lunn, N. Best, A. Thomas, J. Wakefield, and D. Spiegelhalter. Bayesian analysis of population pk/pd models: general concepts and software. *Journal of pharmacokinetics and pharmacodynamics*, 29(3):271–307, 2002. doi: 10.1023/A:1020206907668.
- E. Maheux, I. Koval, J. Ortholand, C. Birkenbihl, D. Archetti, V. Bouteloup, S. Epelbaum, C. Dufouil, M. Hofmann-Apitius, and S. Durrleman. Forecasting individual progression trajectories in alzheimer’s disease. *Nature Communications*, 14(1):761, 2023. doi: 10.1038/s41467-022-35712-5.
- M. D. McKay, R. J. Beckman, and W. J. Conover. A comparison of three methods for selecting values of input variables in the analysis of output from a computer code. *Technometrics*, 21(2):239–245, 1979. doi: 10.1080/00401706.1979.10489755.
- B. McMahan, E. Moore, D. Ramage, S. Hampson, and B. A. y Arcas. Communication-efficient learning of deep networks from decentralized data. In *Artificial Intelligence and Statistics*, pages 1273–1282. PMLR, 2017.
- W. Q. Meeker and L. A. Escobar. Teaching about approximate confidence regions based on maximum likelihood estimation. *The American Statistician*, 49(1):48–53, 1995. doi: 10.1080/00031305.1995.10476112.
- P. K. Mogensen and A. N. Riseth. Optim: A mathematical optimization package for Julia. *Journal of Open Source Software*, 3(24):615, 2018. doi: 10.21105/joss.00615.
- D. R. Mould and R. N. Upton. Basic concepts in population modeling, simulation, and model-based drug development. *CPT: pharmacometrics & systems pharmacology*, 1(9):1–14, 2012. doi: 10.1038/psp.2012.4.
- S. Muff, J. Signer, and J. Fieberg. Accounting for individual-specific variation in habitat-selection studies: Efficient estimation of mixed-effects models using bayesian or frequentist computation. *Journal of Animal Ecology*, 89(1):80–92, 2020. doi: 10.1111/1365-2656.13087.
- C. Ngufor, H. Van Houten, B. S. Caffo, N. D. Shah, and R. G. McCoy. Mixed effect machine learning: A framework for predicting longitudinal change in hemoglobin a1c. *Journal of Biomedical Informatics*, 89:56–67, 2019. doi: 10.1016/j.jbi.2018.09.001.
- A. Pal. *Lux: Explicit Parameterization of Deep Neural Networks in Julia*, 2023. URL <https://doi.org/10.5281/zenodo.7808904>.
- G. Papamakarios, E. Nalisnick, D. J. Rezende, S. Mohamed, and B. Lakshminarayanan. Normalizing flows for probabilistic modeling and inference. *Journal of Machine Learning Research*, 22(57):1–64, 2021.

- M. Philipps, N. Schmid, and J. Hasenauer. Current state and open problems in universal differential equations for systems biology. *npj Systems Biology and Applications*, 11(1):101, 2025. doi: 10.1038/s41540-025-00550-w.
- J. Pinheiro, D. Bates, S. DebRoy, D. Sarkar, R. C. Team, et al. Linear and nonlinear mixed effects models. *R package version*, 3(57):1–89, 2007.
- J. C. Pinheiro and D. M. Bates. Approximations to the log-likelihood function in the nonlinear mixed-effects model. *Journal of Computational and Graphical Statistics*, 4(1):12–35, 1995. doi: 10.1080/10618600.1995.10474663.
- J. C. Pinheiro and D. M. Bates. *Mixed-Effects Models in S and S-PLUS*. Springer-Verlag, New York, 2000. doi: 10.1007/b98882.
- J. C. Pinheiro and E. C. Chao. Efficient laplacian and adaptive gaussian quadrature algorithms for multilevel generalized linear mixed models. *Journal of Computational and Graphical Statistics*, 15(1):58–81, 2006. doi: 10.1198/106186006x96962.
- M. J. Powell et al. The bobyqa algorithm for bound constrained optimization without derivatives. *Cambridge NA Report NA2009/06, University of Cambridge, Cambridge*, 26(26-46): 1, 2009.
- PumasAI. *SimpleChains.jl: Fast and Simple Neural Networks in Julia*, 2022. URL <https://github.com/PumasAI/SimpleChains.jl>.
- L. R. Rabiner. A tutorial on hidden Markov models and selected applications in speech recognition. *Proceedings of the IEEE*, 77(2):257–286, 1989. doi: 10.1109/5.18626.
- C. Rackauckas and Q. Nie. DifferentialEquations.jl – a performant and feature-rich ecosystem for solving differential equations in Julia. *Journal of Open Research Software*, 5(1):15, 2017. doi: 10.5334/jors.151.
- C. Rackauckas, Y. Ma, J. Martensen, C. Warner, K. Zubov, R. Supekar, D. Skinner, A. Ramadhan, and A. Edelman. Universal differential equations for scientific machine learning. *arXiv preprint arXiv:2001.04385*, 2020a.
- C. Rackauckas, Y. Ma, A. Noack, V. Dixit, P. K. Mogensen, S. Byrne, S. Maddhashiya, J. B. Santiago Calderón, J. Nyberg, J. V. Gobburu, et al. Accelerated predictive healthcare analytics with pumas, a high performance pharmaceutical modeling and simulation platform. *BioRxiv*, pages 2020–11, 2020b. doi: 10.1101/2020.11.28.402297.
- A. Raue, C. Kreutz, T. Maiwald, J. Bachmann, M. Schilling, U. Klingmüller, and J. Timmer. Structural and practical identifiability analysis of partially observed dynamical models by

- exploiting the profile likelihood. *Bioinformatics*, 25(15):1923–1929, 2009. doi: 10.1093/bioinformatics/btp358.
- J. Revels, M. Lubin, and T. Papamarkou. Forward-mode automatic differentiation in julia. *arXiv preprint arXiv:1607.07892*, 2016.
- D. J. Rezende and S. Mohamed. Variational inference with normalizing flows. In *International Conference on Machine Learning*, pages 1530–1538. PMLR, 2015.
- F. Rijmen, F. Tuerlinckx, P. De Boeck, and P. Kuppens. A nonlinear mixed model framework for item response theory. *Psychological methods*, 8(2):185, 2003. doi: 10.1037/1082-989x.8.2.185.
- C. P. Robert and G. Casella. *Monte Carlo Statistical Methods*, volume 2. Springer-Verlag, 2004.
- R. M. Savic and M. O. Karlsson. Importance of shrinkage in empirical Bayes estimates for diagnostics: Problems and solutions. *The AAPS Journal*, 11(3):558–569, 2009. doi: 10.1208/s12248-009-9133-0.
- S. Schliehe-Diecks, P. Kappeler, and R. Langrock. On the application of mixed hidden markov models to multiple behavioural time series. *Interface focus*, 2(2):180–189, 2012. doi: 10.1098/rsfs.2011.0077.
- L. B. Sheiner and S. L. Beal. Evaluation of methods for estimating population pharmacokinetic parameters. i. michaelis-menten model: routine clinical pharmacokinetic data. *Journal of pharmacokinetics and biopharmaceutics*, 8(6):553–571, 1980. doi: 10.1007/BF01060053.
- F. Sigrist. Latent gaussian model boosting. *IEEE Transactions on Pattern Analysis and Machine Intelligence*, 45(2):1894–1905, 2022. doi: 10.1109/TPAMI.2022.3168152.
- Simulations Plus. Monolix 2024r1, 2024. URL <https://www.simulations-plus.com/software/monolix/>. Nonlinear mixed effects modelling software for pharmacometrics.
- Stan Development Team. RStan: the R interface to Stan, 2026. URL <https://mc-stan.org/>. R package version 2.39.0.
- M. Tarek and P. Afonso. Fitting large nonlinear mixed effects models using variational expectation maximization. *arXiv preprint arXiv:2604.26160*, 2026.
- L. Tierney and J. B. Kadane. Accurate approximations for posterior moments and marginal densities. *Journal of the American Statistical Association*, 81(393):82–86, 1986. doi: 10.1080/01621459.1986.10478240.

- A. W. van der Vaart. *Asymptotic Statistics*. Cambridge Series in Statistical and Probabilistic Mathematics. Cambridge University Press, Cambridge, 1998. doi: 10.1017/CBO9780511802256.
- L. von Bertalanffy. Quantitative laws in metabolism and growth. *The Quarterly Review of Biology*, 32(3):217–231, 1957. doi: 10.1086/401873.
- J. Wakefield. The bayesian analysis of population pharmacokinetic models. *Journal of the American Statistical Association*, 91(433):62–75, 1996. doi: 10.1080/01621459.1996.10476664.
- C. Wang, M. Y. Peeters, K. Allegaert, H. J. Blussé van Oud-Alblas, E. H. Krekels, D. Tibboel, M. Danhof, and C. A. Knibbe. A bodyweight-dependent allometric exponent for scaling clearance across the human life-span. *Pharmaceutical Research*, 29(6):1570–1581, 2012. doi: 10.1007/s11095-012-0668-x.
- Y. Wang. Derivation of various nonmem estimation methods. *Journal of Pharmacokinetics and pharmacodynamics*, 34(5):575–593, 2007. doi: 10.1007/s10928-008-9083-7.
- G. C. Wei and M. A. Tanner. A monte carlo implementation of the em algorithm and the poor man’s data augmentation algorithms. *Journal of the American Statistical Association*, 85(411):699–704, 1990. doi: 10.1080/01621459.1990.10474930.
- H. White. Maximum likelihood estimation of misspecified models. *Econometrica: Journal of the econometric society*, pages 1–25, 1982. doi: 10.2307/1912526.
- R. C. Wilson, O. W. Butters, D. Avraam, J. Baker, J. A. Tedds, A. Turner, M. Murtagh, and P. R. Burton. Datashield – new directions and dimensions. *Data Science Journal*, 16: 21, 2017. doi: 10.5334/dsj-2017-021.
- T. Wörtwein, N. B. Allen, L. B. Sheeber, R. P. Auerbach, J. F. Cohn, and L.-P. Morency. Neural mixed effects for nonlinear personalized predictions. In *Proceedings of the 25th International Conference on Multimodal Interaction*, pages 445–454, 2023. doi: 10.1145/3577190.3614115.
- W. Zucchini, I. L. MacDonald, and R. Langrock. *Hidden Markov Models for Time Series: An Introduction Using R*. Chapman & Hall/CRC, Boca Raton, 2nd edition, 2016. doi: 10.1201/b20790.

A Further modeling features

This appendix develops five features that the main text summarized: random effects at several grouping levels, multiple observations per individual, censored observations, Markov observation models, and the recording of doses and events. The first four extend the conditional model or the random-effect structure of Section 2 while leaving the estimation machinery of Section 2.4 unchanged, and the last describes how interventions are encoded in the data table that binds a model to its data.

A.1 Nested random effects

For clarity, the main text considers a single random-effect grouping variable, e.g., the individual level. Many applications are hierarchical, however, with variability arising at multiple grouping levels, such as individuals nested within sites or studies. **NoLimits.jl** supports such structures by associating each random effect with its own grouping factor.

Consider individuals $i \in \mathcal{I}_s$ nested within sites $s = 1, \dots, S$. A site-level random effect U_s is shared by all individuals at a site, while an individual-level random effect B_i varies within sites,

$$U_s \sim p_U(\cdot \mid \theta), \quad (27)$$

$$B_i \sim p_B(\cdot \mid \theta), \quad i \in \mathcal{I}_s, \quad (28)$$

$$Y_{i,j} \mid U_s = u_s, B_i = b_i \sim p_{Y|U,B}(\cdot \mid u_s, b_i, x_i, \theta). \quad (29)$$

The marginal likelihood then factorizes over sites rather than individuals,

$$p_Y(y \mid \theta) = \prod_{s=1}^S \int \left[\prod_{i \in \mathcal{I}_s} \int \prod_j p_{Y|U,B}(y_{i,j} \mid u, b, x_i, \theta) p_B(b \mid \theta) db \right] p_U(u \mid \theta) du. \quad (30)$$

NoLimits.jl supports both nested and crossed grouping factors [Pineiro and Chao, 2006]. The estimators of Section 2.4 extend naturally by operating on the joint random-effect vector associated with each grouping block. For Laplace methods, conditional modes and Hessians are computed jointly over all random effects in a block. For EM-type methods, expectations are taken with respect to the corresponding joint posterior. Full MCMC inference requires only augmenting the hierarchy with the additional random-effect levels and sampling the resulting joint posterior. For ODE-based models, random effects that enter the dynamics must currently be defined at the individual level.

A.2 Multiple measurements

Individuals may contribute multiple outcomes rather than a single response. Let $y_{i,j}^{(r)}$ denote observation j of outcome r for individual i . Conditional on the random effect B_i , the likelihood factorizes as

$$p_{Y|B}(y_i | b_i, x_i, \theta) = \prod_{r=1}^R \prod_j p_{Y|B}^{(r)}(y_{i,j}^{(r)} | b_i, x_i, \theta), \quad (31)$$

where each outcome may follow a different observation model. Sharing the random effect across outcomes induces dependence between them and enables joint modeling. Since only the conditional likelihood changes, all estimators of Section 2.4 apply without modification. In **NoLimits.jl**, multiple outcomes are specified through separate observation formulas, with missing measurements represented as `missing`.

A.3 Censored measurements

Censored measurements arise when the exact observation is unknown but is known to lie within an interval, for example below a lower limit of quantification. Let $[\ell_{i,j}, u_{i,j}]$ denote the censoring interval for observation j of individual i . Instead of contributing a density, a censored observation contributes the corresponding interval probability,

$$P(\ell_{i,j} \leq Y_{i,j} \leq u_{i,j} | B_i = b_i, x_i, \theta) = P_{Y|B}(u_{i,j} | b_i, x_i, \theta) - P_{Y|B}(\ell_{i,j} | b_i, x_i, \theta), \quad (32)$$

where $P_{Y|B}$ denotes the conditional cumulative distribution function. The conditional likelihood is obtained by replacing censored observations with these interval probabilities, and the resulting likelihood is marginalized over the random effects as in Equation 6.

Likelihood-based estimators evaluate this likelihood directly, whereas stochastic estimators such as MCEM and SAEM treat censored observations as latent variables and sample them from the corresponding truncated observation model [Wei and Tanner, 1990]. In **NoLimits.jl**, censoring is specified by wrapping the observation distribution and providing censoring limits as constants or covariates.

A.4 Markov observation models

NoLimits.jl implements a family of Markov observation models that covers discrete and continuous time, hidden and directly observed states, univariate and multivariate emissions, and coarsened state observations (Table S1). For observed-state models the conditional density $p_{Y|B}(y_i | b_i, x_i, \theta)$ of Equation 2 is a product of transition probabilities and is available in closed form. For an HMM it is instead obtained by a recursion over an unobserved

Outcome distribution	Time	States	Observation
DiscreteTimeDiscreteStatesHMM	Discrete	Hidden	Univariate emission
ContinuousTimeDiscreteStatesHMM	Continuous	Hidden	Univariate emission
MVDiscreteTimeDiscreteStatesHMM	Discrete	Hidden	Multivariate emissions with missing entries
MVContinuousTimeDiscreteStatesHMM	Continuous	Hidden	Multivariate emissions with missing entries
DiscreteTimeObservedStatesMarkovModel	Discrete	Observed	State label
ContinuousTimeObservedStatesMarkovModel	Continuous	Observed	State label
CoarsedObservedStatesMarkovModel	Both	Observed	Set of compatible state labels

Supplementary Table S1: Markov-model outcome distributions available in **NoLimits.jl**, including hidden- and observed-state models, discrete- and continuous-time variants, multivariate extensions, and coarsened-state observations.

within-subject state sequence [Rabiner, 1989, Zucchini et al., 2016]. Let the latent states $Z_{i,1}, \dots, Z_{i,n_i}$ be random variables taking values in $\{1, \dots, K\}$ with initial distribution π , transition matrices $\mathbf{P}_{i,j}$ that may depend on the covariates, the time, and the random effect, and state-conditional emission densities $p_{Y|Z}(y_{i,j} | z_{i,j}, x_{i,j}, \theta)$. The conditional likelihood is computed by the forward recursion

$$\begin{aligned}
\alpha_{i,1}(k) &= \pi_k p_{Y|Z}(y_{i,1} | k, x_{i,1}, \theta), \\
\alpha_{i,j}(l) &= \left[\sum_{k=1}^K \alpha_{i,j-1}(k) [\mathbf{P}_{i,j}]_{kl} \right] p_{Y|Z}(y_{i,j} | l, x_{i,j}, \theta), \\
p_{Y|B}(y_i | b_i, x_i, \theta) &= \sum_{k=1}^K \alpha_{i,n_i}(k),
\end{aligned} \tag{33}$$

which enters the joint and marginal densities of Equations 4 and 6 in place of a closed-form term, so that every estimator of Section 2.4 applies without change. In the continuous-time variants the transition matrices are obtained as matrix exponentials of a rate matrix. The transition matrix may be parameterized by a neural network mapped through a row-wise softmax and the most likely hidden-state sequence is recovered by Viterbi decoding.

For example, an HMM with two hidden states is defined as follows.

```
model = @Model begin
```

```

@fixedEffects begin
  p12 = RealNumber(0.1, scale = :logit)
  p21 = RealNumber(0.2, scale = :logit)
  mu1 = RealNumber(0.0)
  mu2 = RealNumber(3.0)
  sigma = RealNumber(0.5, scale = :log)
end
@formulas begin
  P = [1 - p12      p12;
       p21      1 - p21]
  y ~ DiscreteTimeDiscreteStatesHMM(P,
    (Normal(mu1, sigma), Normal(mu2, sigma)),
    Categorical([0.5, 0.5]))
end
end

```

The three arguments of `DiscreteTimeDiscreteStatesHMM` specify the transition matrix, the state-specific emission distributions, and the initial state distribution. While this explicit construction is convenient for small state spaces, larger models can declare the full transition matrix and initial distribution directly using the `DiscreteTransitionMatrix` and `ProbabilityVector` parameters of Table 2. For continuous-time models, the transition structure is instead supplied as the rate matrix `ContinuousTransitionMatrix`.

A.5 Laplace and FOCEI approximation

Let

$$g_i(b) = \log p_{Y|B}(y_i | b, x_i, \theta) + \log p_B(b | x_i, \theta), \quad (34)$$

so that the marginal likelihood contribution of individual i is $\int_{\mathcal{B}} \exp(g_i(b)) db$. A second-order Taylor expansion around the EBE \hat{b}_i yields

$$g_i(b) \approx g_i(\hat{b}_i) + \frac{1}{2}(b - \hat{b}_i)^\top H_i(\theta)(b - \hat{b}_i), \quad H_i(\theta) = \nabla_b^2 g_i(b) \Big|_{b=\hat{b}_i}, \quad (35)$$

where the first-order term vanishes because \hat{b}_i is a mode. Substituting this approximation into the marginal integral yields the Laplace approximation of Equation 11 [Tierney and Kadane, 1986].

The FOCEI approximation uses the same form but replaces the exact Hessian by the curvature implied by a first-order linearization of the conditional model around \hat{b}_i [Wang, 2007, Pinheiro and Chao, 2006]. Letting $\phi_{ij}(b)$ denote the parameters of the observation distribution for observation j of individual i , FOCEI approximates the curvature of the conditional

log-likelihood by its Fisher information [Fisher, 1925] while retaining the exact curvature of the random-effects distribution,

$$H_i(\theta) = -\sum_{j=1}^{n_i} J_{ij}^\top \mathcal{I}(\phi_{ij}) J_{ij} + \nabla_b^2 \log p_B(\hat{b}_i | x_i, \theta), \quad J_{ij} = \left. \frac{\partial \phi_{ij}}{\partial b} \right|_{b=\hat{b}_i}, \quad (36)$$

where $\mathcal{I}(\phi_{ij})$ is the Fisher information of the observation distribution and J_{ij} is the Jacobian of its parameters with respect to the random effects. For bounded random-effect domains, the Gaussian integral is evaluated over the corresponding support rather than over \mathbb{R}^{n_b} [Greenberg, 2013].

Gradient via the envelope theorem. Gradient-based optimization of θ requires the gradient of the approximate marginal log-likelihood. Making the dependence on θ explicit and taking the logarithm of Equation 11, the per-individual approximate marginal log-likelihood is

$$\ell_i(\theta) = g_i(\hat{b}_i(\theta), \theta) - \frac{1}{2} \log \det(-H_i(\theta)) + \frac{n_b}{2} \log(2\pi), \quad (37)$$

where $\hat{b}_i(\theta) = \arg \max_b g_i(b, \theta)$ is the EBE and $H_i(\theta) = \nabla_b^2 g_i(b, \theta)|_{b=\hat{b}_i}$. Both $\hat{b}_i(\theta)$ and $H_i(\theta)$ depend on θ , so a naive total derivative would have to differentiate through the inner optimization. The envelope theorem removes this for the first term, because $\hat{b}_i(\theta)$ maximizes $g_i(\cdot, \theta)$ the inner gradient $\nabla_b g_i(\hat{b}_i, \theta)$ vanishes, and the total derivative of $g_i(\hat{b}_i(\theta), \theta)$ reduces to its explicit partial $\nabla_\theta g_i(\hat{b}_i, \theta)$. The log-determinant term is not stationary in b , so its total derivative retains the sensitivity of the mode,

$$\nabla_\theta \ell_i(\theta) = \nabla_\theta g_i(\hat{b}_i, \theta) - \frac{1}{2} \left[\nabla_\theta \log \det(-H_i) + \left(\nabla_b \log \det(-H_i) \right)^\top \frac{d\hat{b}_i}{d\theta} \right], \quad (38)$$

where the partial derivatives of the log-determinant treat b and θ as independent. The mode sensitivity follows from the implicit function theorem applied to the optimality condition $\nabla_b g_i(\hat{b}_i(\theta), \theta) = 0$,

$$\frac{d\hat{b}_i}{d\theta} = \left(-H_i(\theta) \right)^{-1} \nabla_\theta \nabla_b g_i(\hat{b}_i, \theta). \quad (39)$$

NoLimits.jl evaluates Equations 38 and 39 by automatic differentiation of g_i and $\log \det(-H_i)$ at the converged mode, reusing the Cholesky factor of $-H_i(\theta)$ already formed for Equation 11. The same identities apply to FOCEI with the respective approximation of the hessian term (Equation 36).

A.6 EM algorithm and Monte Carlo expectation

The EM algorithm constructs the surrogate objective $Q(\theta | \theta_t)$ of Equation 12, whose maximization guarantees non-decreasing marginal likelihood values [Dempster et al., 1977]. For

nonlinear and non-Gaussian models, the required expectation is generally intractable. MCEM therefore approximates it using samples $b_i^{(1)}, \dots, b_i^{(M_t)}$ from the posterior distribution of Equation 8,

$$Q(\theta | \theta_t) \approx \sum_{i=1}^N \frac{1}{M_t} \sum_{m=1}^{M_t} \log p_{Y,B}(y_i, b_i^{(m)} | x_i, \theta). \quad (40)$$

In **NoLimits.jl**, these samples are obtained through **Turing.jl**, typically using Metropolis–Hastings or NUTS sampling to target the posterior distribution of Equation 8 [Robert and Casella, 2004, Chib and Greenberg, 1995].

A.7 SAEM learning-rate schedule

The SAEM learning rate γ_k controls the update of the sufficient statistics of Equation 14 at iteration k . **NoLimits.jl** uses a piecewise schedule consisting of an optional burn-in, an initial plateau, and two polynomial decay phases,

$$\gamma_k = \begin{cases} 0, & 1 \leq k \leq K_{\text{burn}}, \\ 1, & K_{\text{burn}} < k \leq K_{\text{burn}} + K_0, \\ k^{-a_1}, & K_{\text{burn}} + K_0 < k \leq K_{\text{burn}} + K_0 + K_1, \\ \left(k - K_{\text{offset}} + \gamma_{K_{\text{offset}}}^{-1/a_2}\right)^{-a_2}, & k > K_{\text{burn}} + K_0 + K_1, \end{cases} \quad (41)$$

where

$$K_{\text{offset}} = K_{\text{burn}} + K_0 + K_1. \quad (42)$$

The first phase performs no updates, the second uses full updates, and the final two phases gradually reduce the learning rate. The last branch ensures a continuous transition between the two decay regimes while preserving polynomial decay. For $a_1, a_2 \in (0.5, 1]$, the schedule satisfies the Robbins–Monro conditions required for stochastic approximation convergence.

A.8 SAEM sufficient-statistic update

Suppose the complete-data density belongs to an exponential family,

$$\log p_{Y,B}(y_i, b | x_i, \theta) = \langle \phi(\theta), T(y_i, b) \rangle - \psi(\theta) + \text{const}, \quad (43)$$

where T is a sufficient statistic, $\phi(\theta)$ the natural parameter, and $\psi(\theta)$ the log-partition function. The surrogate of Equation 12 then depends on θ only through the expected sufficient statistics. SAEM replaces these expectations by the stochastic recursion

$$\bar{T}^{(t)} = (1 - \gamma_t) \bar{T}^{(t-1)} + \gamma_t \sum_{i=1}^N \frac{1}{M_t} \sum_{s=1}^{M_t} T(y_i, b_i^{(t,s)}), \quad (44)$$

where $b_i^{(t,s)}$ are samples from the conditional distribution of the random effects. The maximization step then updates the parameters by maximizing

$$\langle \phi(\theta), \bar{T}^{(t)} \rangle - N\psi(\theta), \quad (45)$$

which is available in closed form for common exponential-family models such as Gaussian random effects [Kuhn and Lavielle, 2005, Comets et al., 2017].

In **NoLimits.jl**, the random-effect samples are generated by the default **SaemixMH** sampler, a lightweight Metropolis–Hastings scheme inspired by **saemix** [Comets et al., 2017] that avoids constructing a full **Turing.jl** model at each iteration.

A.9 Prediction

This appendix gives the predictors summarized in Section 2.6, which depend on whether the individual was observed during model fitting.

Individuals observed in training. For an individual included in the training data, the observed responses y_i inform the posterior of the random effect in Equation 8. A computationally inexpensive prediction at covariate value x_i , possibly a new value or time point, substitutes the corresponding EBE \hat{b}_i into the conditional mean,

$$\hat{y}_i = \mathbb{E}(Y_i \mid B_i = \hat{b}_i, x_i, \theta), \quad (46)$$

whereas propagating the uncertainty in the random effect averages the conditional mean over the posterior,

$$\hat{y}_i = \int_{\mathcal{B}} \mathbb{E}(Y_i \mid B_i = b, x_i, \theta) p_{B|Y}(b \mid y_i, x_i, \theta) db, \quad (47)$$

which reduces to the plug-in predictor of Equation 46 when the conditional mean is linear in the random effect [Lindstrom and Bates, 1990].

Individuals not observed in training. For an unseen individual, no posterior distribution is available and two prediction strategies arise. The first is the plug-in predictor, which replaces the random effect by its covariate-dependent prior mean,

$$\hat{y}_i = \mathbb{E}(Y_i \mid B_i = \mathbb{E}(B_i \mid x_i, \theta), x_i, \theta), \quad (48)$$

while the second is the marginal predictor,

$$\hat{y}_i = \int_{\mathcal{B}} \mathbb{E}(Y_i \mid B_i = b, x_i, \theta) p_B(b \mid x_i, \theta) db, \quad (49)$$

which corresponds to the population mean implied by the marginal model in Equation 6 [Lavielle, 2014]. The two predictors coincide when the conditional mean is linear in the random effects and generally differ otherwise.

A.10 Numerical configuration

Beyond the optimizer and parameter transformations of Section 4, two further numerical components are configured separately from the model and its data binding, the multistart procedure and the ODE solver.

Multistart. To improve robustness against local optima, any optimization-based estimator can be wrapped in the `Multistart` procedure, which draws starting points from user-specified distributions either independently or through Latin hypercube sampling (LHS) [McKay et al., 1979]. Candidate starts are first ranked by a cheap screening objective and only the most promising are fully optimized, controlled by `n_draws_requested` and `n_draws_used`, and the wrapper is combined with an estimator by passing it as the first argument to `fit_model`.

```
ms = Multistart(dists = (beta1 = Normal(0.0, 1.0),
                       beta2 = Normal(1.0, 0.5)),
               n_draws_requested = 200, n_draws_used = 50,
               sampling = :lhs)
res = fit_model(ms, dm, Laplace())
best_fit = get_multistart_best(res)
plot_multistart_waterfall(res)
```

Fixed effects without a sampling distribution are held at their initial values, the best fit is recovered with `get_multistart_best`, and the spread of objective values across starts is summarized by the multistart waterfall plot.

ODE solver configuration. ODE solver settings are configured separately from the model specification using the function `set_solver_config`. This keeps the numerical integrator independent of both the data binding and the estimation method. By default, **NoLimits.jl** uses `Tsit5()`, but any solver from **OrdinaryDiffEq.jl** can be supplied, including stiff solvers, together with solver-specific options such as `abstol` (and `reltol`), which are forwarded to the ODE solver. For example,

```
model = set_solver_config(model; alg = Tsit5(), kwargs = (; abstol = 1e-8))
```

configures the model to use the explicit `Tsit5()` solver with a tighter absolute tolerance. As with all configuration functions in **NoLimits.jl**, the call returns an updated `Model` object rather than modifying its argument in place.

B Additional model specifications and diagnostics

B.1 Warfarin diagnostics

This appendix reports convergence and inter-individual-variability diagnostics for the warfarin analysis of Section 6.1, together with the marginal posteriors of the variance components from its Bayesian fit.

B.1.1 Convergence

Convergence of the MCEM fit is assessed from the per-iteration trajectories of the parameters and surrogate objective Q , obtained with `plot_em_trajectories`:

```
plot_em_trajectories(fit; ncols = 3, style = my_style)
```

Figure S1 shows stable parameter estimates and a plateauing Q -function after roughly 20 iterations, indicating convergence. The absorption-rate parameter `ka_mean` exhibits the largest Monte Carlo variability, consistent with its wider confidence interval.

B.1.2 Inter-individual variability

Figure S2 compares the fitted random-effects distributions with the corresponding EBEs. For V , the individual estimates closely follow the population distribution (Figure S2B), whereas the `ka` estimates are more concentrated around the population mean (Figure S2A), indicating shrinkage.

Shrinkage, defined in Section 2.7, is quantified with `compute_shrinkage`:

```
shrink = compute_shrinkage(fit)
```

yielding

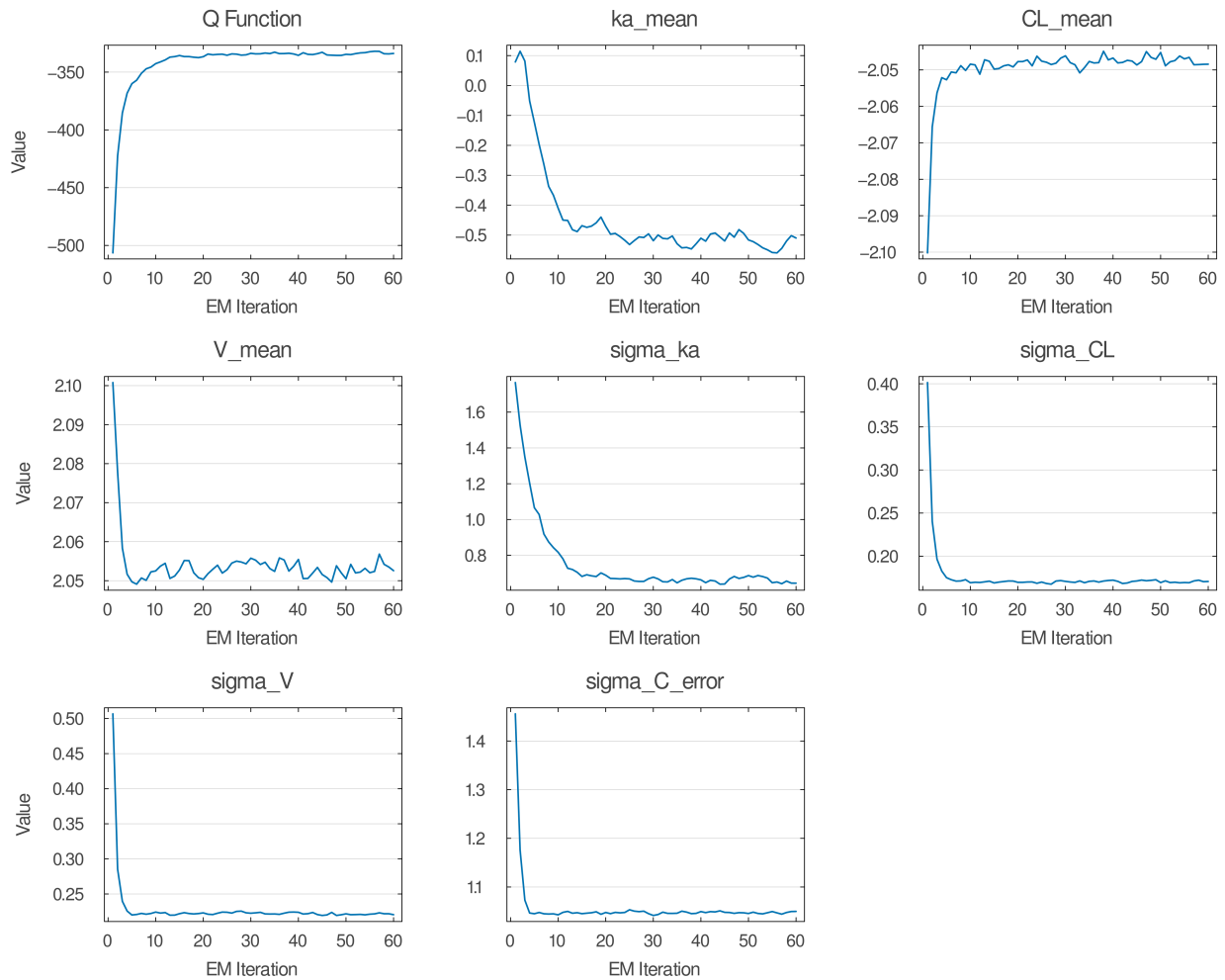
ETA shrinkage

ka : 42.9%

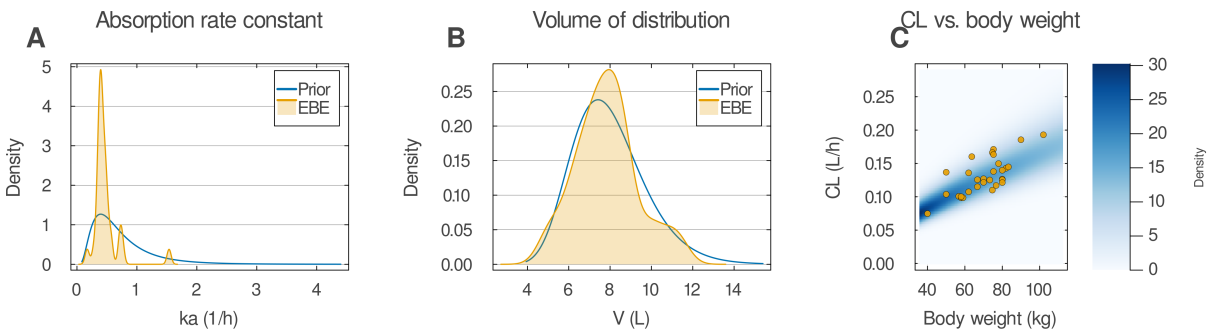
CL : 15.6%

V : 11.7%

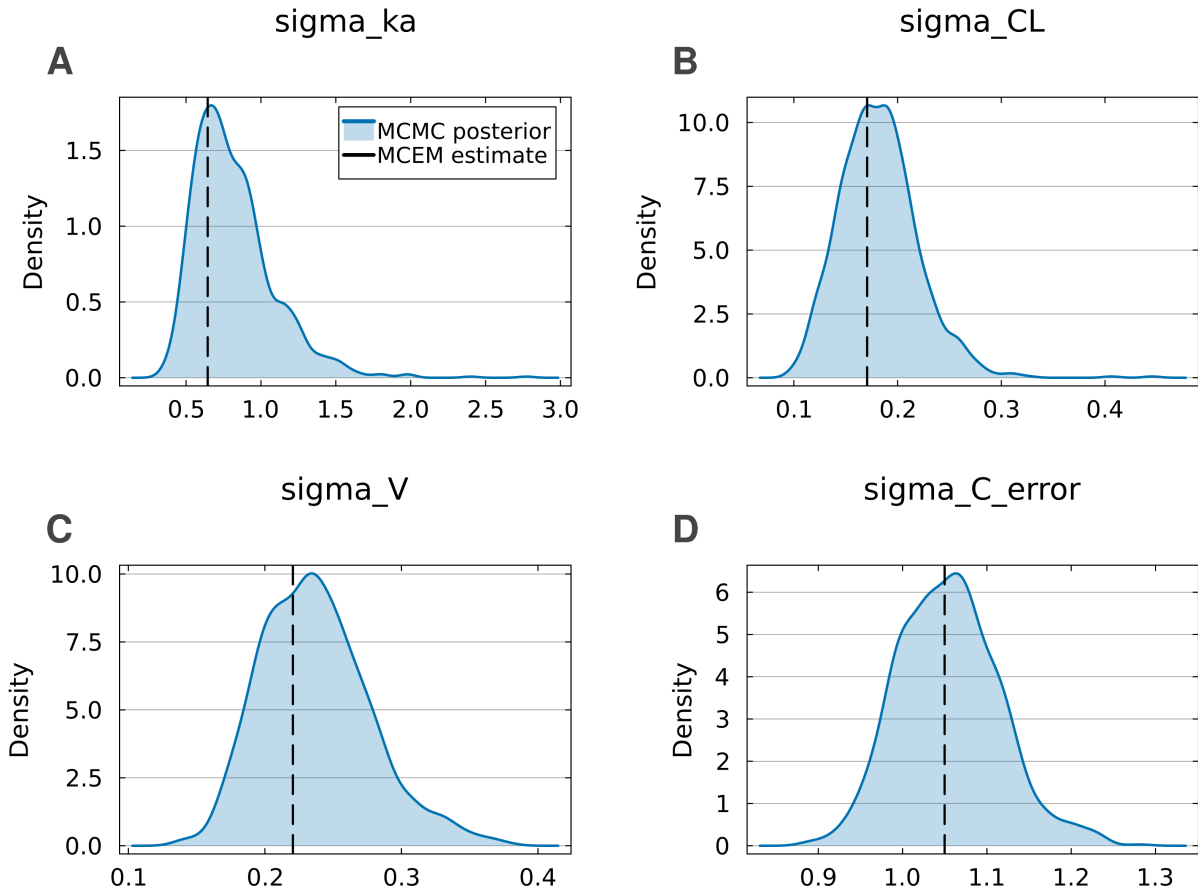
The absorption-rate parameter `ka` exhibits substantial shrinkage (42.9%), exceeding the conventional 30% threshold [Savic and Karlsson, 2009] and reflecting the limited information in the absorption phase. In contrast, `CL` and `V` show low shrinkage (15.6% and 11.7%), indicating that the elimination phase provides sufficient individual information. Figure S2C also confirms the expected increase of clearance with body weight under the allometric model.



Supplementary Figure S1: MCEM convergence trajectories for the warfarin model: the Q-function (upper left) and all fixed-effect parameters.



Supplementary Figure S2: Inter-individual variability diagnostics. (A) Population prior and KDE of EBEs for ka . (B) Same for V . (C) Conditional distribution of CL as a function of body weight with individual EBEs overlaid.



Supplementary Figure S3: Marginal posterior distributions of the random-effect standard deviations and the residual standard deviation from the Bayesian fit of the warfarin model, with the corresponding MCEM point estimates as dashed lines: (A) σ_{k_a} , (B) σ_{CL} , (C) σ_V , (D) σ_C .

B.1.3 Posterior distributions of the standard deviations

Figure S3 compares the posteriors of the four standard-deviation parameters from the Bayesian fit of Section 6.1.5 with their MCEM point estimates. Each estimate lies close to the mode of its posterior. The standard deviations of clearance, volume, and the residual error have tight posteriors, whereas the absorption-rate standard deviation σ_{k_a} has a broader, right-skewed posterior, mirroring the behavior of μ_{k_a} .

B.2 Parametric pharmacodynamic reference model

The PD example of Section 6.2 compares two learnable concentration-effect functions against a parametric saturable **E_{max}** reference. The neural-network and soft-tree models are listed in

full in that section. For completeness, the `@Model` specification of the parametric reference is given here. It shares the PK submodel, random-effects structure, and observation model of the neural-network model, differing only in the fixed effects and the effect function. The fixed effects carry the saturable parameters `Emax` and `EC50` in place of the learnable `m1_params`, and the effect enters the turnover model of Equation 20 through the saturable form of Equation 21 rather than a learned function:

```

model_par = @Model begin
  @fixedEffects begin
    ka_mean    = RealNumber(0.0); CL_mean    = RealNumber(-2.0)
    V_mean     = RealNumber(2.0); kout_mean  = RealNumber(-3.0)
    sigma_ka   = RealNumber(0.3, scale = :log)
    sigma_CL   = RealNumber(0.3, scale = :log)
    sigma_V    = RealNumber(0.3, scale = :log)
    sigma_C    = RealNumber(1.0, scale = :log)
    sigma_kout = RealNumber(0.3, scale = :log)
    sigma_R    = RealNumber(5.0, scale = :log)
    Emax       = RealNumber(1.0, scale = :log)
    EC50       = RealNumber(1.0, scale = :log)
  end
  @covariates begin
    t = Covariate()
    d = ConstantCovariate(; constant_on = :id)
    wt = ConstantCovariate(; constant_on = :id)
    R0 = ConstantCovariate(; constant_on = :id)
  end
  @randomEffects begin
    ka = RandomEffect(LogNormal(ka_mean, sigma_ka); column = :id)
    CL = RandomEffect(
      LogNormal(CL_mean + 0.75 * log(wt / 70.0), sigma_CL);
      column = :id)
    V = RandomEffect(LogNormal(V_mean, sigma_V); column = :id)
    kout = RandomEffect(LogNormal(kout_mean, sigma_kout); column = :id)
  end
  @DifferentialEquation begin
    eff(t) = Emax * (center / V) / (EC50 + center / V)
    D(depot) ~ -ka * depot
    D(center) ~ ka * depot - (CL / V) * center
    D(response) ~ kout * (R0 - response * (1 + eff(t)))
  end
end

```

```
end
@initialDE begin
    depot = d; center = 0.0; response = R0
end
@formulas begin
    C ~ Normal(center(t) / V, sigma_C); R ~ Normal(response(t), sigma_R)
end
end
```

The cross-validated comparison of Section 6.2 fits this model with the same `fit_cv` call used for the learnable variants, so all three effect models are estimated and scored under an identical protocol.